Response of Jupiter's and Saturn's auroral activity to the solar wind

J. T. Clarke,[1] J. Nichols,[1] J.-C. Gérard,[2] D. Grodent,[2] K. C. Hansen,[3] W. Kurth,[4] G. R. Gladstone,[5] J. Duval,[1] S. Wannawichian,[1] E. Bunce,[6] S. W. H. Cowley,[6] F. Crary,[5] M. Dougherty,[7] L. Lamy,[8] D. Mitchell,[9] W. Pryor,[10] K. Retherford,[5] T. Stallard,[6] B. Zieger,[3] P. Zarka,[8] and B. Cecconi[8]

Received 21 August 2008; revised 6 February 2009; accepted 2 March 2009; published 19 May 2009.

[1] While the terrestrial aurorae are known to be driven primarily by the interaction of the Earth's magnetosphere with the solar wind, there is considerable evidence that auroral emissions on Jupiter and Saturn are driven primarily by internal processes, with the main energy source being the planets' rapid rotation. Prior observations have suggested there might be some influence of the solar wind on Jupiter's aurorae and indicated that auroral storms on Saturn can occur at times of solar wind pressure increases. To investigate in detail the dependence of auroral processes on solar wind conditions, a large campaign of observations of these planets has been undertaken using the Hubble Space Telescope, in association with measurements from planetary spacecraft and solar wind conditions both propagated from 1 AU and measured near each planet. The data indicate a brightening of both the auroral emissions and Saturn kilometric radiation at Saturn close in time to the arrival of solar wind shocks and pressure increases, consistent with a direct physical relationship between Saturnian auroral processes and solar wind conditions. At Jupiter the correlation is less strong, with increases in total auroral power seen near the arrival of solar wind forward shocks but little increase observed near reverse shocks. In addition, auroral dawn storms have been observed when there was little change in solar wind conditions. The data are consistent with some solar wind influence on some Jovian auroral processes, while the auroral activity also varies independently of the solar wind. This extensive data set will serve to constrain theoretical models for the interaction of the solar wind with the magnetospheres of Jupiter and Saturn.

Citation: Clarke, J. T., et al. (2009), Response of Jupiter's and Saturn's auroral activity to the solar wind, *J. Geophys. Res.*, *114*, A05210, doi:10.1029/2008JA013694.

1. Introduction

[2] Each planet with a magnetic field and collisionally thick atmosphere displays auroral emissions, produced when charged particles, moving along field lines and accelerated to high energies, impact and excite atmospheric atoms and molecules. The Earth's magnetosphere and auroral processes have been studied in detail for many years, with global auroral brightenings generally resulting from changes in the solar wind that disturb conditions within the magnetosphere.

[3] At Jupiter, Pioneer and Voyager spacecraft data established that the magnetosphere is filled with high-density plasma from volcanic activity at Io. Both observations of the auroral oval latitude compared with auroral emissions from the magnetic footprints of the satellites and theoretical modeling have demonstrated that the main auroral oval maps along the field to a distance about 20–30 Jovian radii (R_J), in the middle magnetosphere far from the solar wind boundary [*Clarke et al.*, 2004]. There is considerable evidence that Jupiter's main auroral oval is driven by outward drifting plasma falling behind corotation, resulting in large field-aligned currents and potentials. While there exists some evidence for a solar wind connection in nonthermal radio emissions [*Barrow et al.*, 1986; *Ladreiter and Leblanc*, 1989; *Kaiser*, 1993; *Prangé et al.*, 1993; *Zarka*, 1998], this middle magnetospheric region far from the solar wind boundary has been proposed to be the main region controlling the auroral emissions [*Hill*, 2004].

[1]Center for Space Physics, Boston University, Boston, Massachusetts, USA.
[2]LPAP, Université de Liège, Liege, Belgium.
[3]AOSS Department, University of Michigan, Ann Arbor, Michigan, USA.
[4]Department of Physics and Astronomy, University of Iowa, Iowa City, Iowa, USA.
[5]Southwest Research Institute, San Antonio, Texas, USA.
[6]Department of Physics and Astronomy, University of Leicester, Leicester, UK.
[7]Blackett Laboratory, Imperial College, London, UK.
[8]LESIA, Observatoire de Paris, UPMC, CNRS, Université Paris Diderot, Meudon, France.
[9]Johns Hopkins University Applied Physics Laboratory, Laurel, Maryland, USA.
[10]Department of Science, Central Arizona College, Coolidge, Arizona, USA.

0148-0227/09/2008JA013694$09.00

[4] At Saturn, the physics of auroral processes is less well understood. Saturn's magnetospheric plasma content (mainly from the rings and icy moons) is much lower than Jupiter's, and the neutral content higher, but the distance to which plasma corotates with the magnetic field fills most of the magnetosphere, like Jupiter and unlike the Earth. Saturn's main auroral activity could be similar to Jupiter's, driven by currents from the enforcement of corotation of outward drifting plasma. Since no emissions have been detected from magnetic footprints of the satellites, there are no direct measurements from UV images of the distance to which the auroral oval maps. There is evidence from both Voyager and Cassini measurements of a Jupiter-like magnetodisc region in Saturn's magnetosphere [*Connerney et al.*, 1983; *Arridge et al.*, 2008], although it is relatively lower density and less stable than at Jupiter. There has been a theoretical prediction that the corotation enforcement currents would be insufficient at Saturn to produce bright auroral emission, and that the main auroral oval must then map close to the solar wind boundary [*Cowley and Bunce*, 2003; *Cowley et al.*, 2003]. Recent measurements with the Cassini spacecraft flying through flux tubes with field-aligned currents lend support to the existence of auroral processes near the solar wind boundary [*Bunce et al.*, 2008]. A centrifugal instability model has also been proposed for Saturn [*Sittler et al.*, 2006], in which auroral brightenings occur during times of magnetospheric compressions due to instabilities in the outer magnetosphere near the outer boundary of the plasma sheet and ring current.

[5] In the case of the Earth's aurorae, detailed ground-based and space-based data have shown that global auroral brightenings can be driven by both a southward turning of the interplanetary magnetic field (IMF) and a pressure pulse associated with a coronal mass ejection (CME) [*Elphinstone et al.*, 1996; *Chua et al.*, 2001]. At the Earth, the coupling between the magnetosphere and the solar wind is particularly strong. When the IMF is southward, magnetic reconnection on the dayside of the magnetosphere creates open flux, and the solar wind motion then drags these flux tubes antisunward. Energy is progressively accumulated in the magnetotail until the growth of an instability in the plasma sheet initiates another process of magnetic reconnection that closes magnetic flux in the tail and releases energy, giving rise to bright auroral emissions. These auroral storms generally begin near midnight, then extend both along the auroral oval and toward the pole. The cycle of ongoing opening and closing of magnetic flux was first proposed by *Dungey* [1961], and it is the underlying idea behind the current understanding of the substorm cycle and magnetospheric convection at the Earth [*Akasofu*, 1964; *McPherron*, 1970; *Siscoe and Huang*, 1985; *Cowley and Lockwood*, 1992].

[6] A solar wind dynamic pressure increase, for example, from a CME, can also be efficient at triggering the formation of a magnetic X line in the tail, and the arrival of such a solar wind pressure increase can result in flux closure and enhanced auroral activity [*Brittnacher et al.*, 2000; *Boudouridis et al.*, 2003; *Meurant et al.*, 2004]. These auroral storms can appear as extended brightenings of the oval, generally starting near noon and extending to the nightside. It has also been shown that a dynamic pressure pulse can directly stimulate the formation of a neutral line and flux closure in the Earth's magnetotail [*Hubert et al.*, 2006]. The changes in Jupiter's and Saturn's auroral emission power discussed below will be most directly comparable to these global changes in auroral activity at the Earth.

[7] Jupiter's and Saturn's magnetospheres are both much larger than the Earth's, and the time scales for disturbances in the solar wind to move from the bow shock past the planet are hours, compared with minutes at the Earth. This longer time scale should correspondingly affect the nature of both internal dynamics and the interaction with the solar wind. At Jupiter, the dense outward drifting plasma reaches a distance where corotation with the magnetic field can no longer be enforced, leading to strong currents in and out of the polar ionosphere and bright auroral emissions [*Hill*, 2001; *Cowley and Bunce*, 2001; *Southwood and Kivelson*, 2001]. Jupiter's total auroral power is more constant than the Earth's, consistent with the steady source of plasma and much larger size of the magnetosphere. Earlier observations of Jupiter's aurorae have shown that a factor of 2 change in the total auroral power is a large deviation from the norm [*Skinner et al.*, 1984; *Livengood et al.*, 1992; *Prangé et al.*, 2001]. The overall brightness of the main oval has also been observed to vary from hour to hour, while generally stable in brightness on time scales of tens of minutes [*Grodent et al.*, 2003a].

[8] There have been a number of reports that Jupiter's auroral emissions may be correlated with solar wind conditions. Observations of Jupiter's near-IR auroral emissions have been compared with solar wind pressure values measured by the Ulysses spacecraft, and a correlation reported between the log of changes in solar wind pressure and total IR auroral power since the prior IR observation [*Baron et al.*, 1996]. These authors proposed that their result supported the "magnetic pumping" hypothesis [*Goertz*, 1978], a process by which charged particles are collectively energized by fluctuations of the magnetic field. A single solar wind event traced from 1 AU has been proposed to correspond to auroral brightenings at both Jupiter and Saturn, within a large uncertainty in the arrival time at the planets and limited coverage of the auroral activity [*Prangé et al.*, 2004]. Evidence exists from two events recorded at the time of the Cassini spacecraft flyby (late 2000 to early 2001) that Jupiter's auroral emissions may brighten at times of solar wind disturbances [*Gurnett et al.*, 2002; *Pryor et al.*, 2005; *Nichols et al.*, 2007], but the data were insufficient to establish the repeatability or the physical nature of the correlation. The observed brightening of the aurora at a time of solar wind pressure increase is opposite to the initial prediction based on the corotation enforcement current system. Increased pressure would reduce the outflow rate of magnetospheric plasma, resulting in weaker currents to enforce corotation and correspondingly fainter auroral emissions [*Southwood and Kivelson*, 2001]. It has since been proposed that an auroral brightening could follow a large solar wind compression by the flywheel effect in the ionosphere (T. Hill and D. Gong, Variations of Jovian and Saturnian auroras induced by changes of solar wind dynamic pressure, paper presented at Magnetospheres of the Outer Planets 2005, University of Leicester, Leicester, U. K.). In addition, a simulation of the effects of large solar wind compressions and relaxations on Jupiter's magnetosphere has indicated that a transient brightening of the

aurora would be expected, at slightly different latitudes depending on the region of enhanced currents, by the same principle of differential rotation rates of the plasma and field [*Cowley et al.*, 2007]. The regions of brightening and the time scales from the campaign reported here can be compared with these theoretical predictions.

[9] While the preceding discussion referred to the total auroral power, Jupiter's aurorae have also shown more localized brightenings, likely reflecting different processes in different regions of the magnetosphere. "Polar flares" [*Waite et al.*, 2001; *Gladstone et al.*, 2002] frequently appear poleward of the main oval near 180° system III longitude, rising to peak brightnesses of tens of MRayleighs in tens of seconds and fading to background over a few minutes. It has been proposed that these events map to the dayside boundary with the solar wind [*Waite et al.*, 2001]. Less often, longer lasting brightenings appear along the main oval at local dawn [*Ballester et al.*, 1996; *Clarke et al.*, 1998; *Grodent et al.*, 2003b; *Gustin et al.*, 2006]. These "dawn storms" brighten over tens of minutes to peak values of several MRayleighs, remain at local dawn while other features in the main oval rotate with the planet, and last a few hours while typically spreading in longitude. These events are not understood, since they occur along the main oval mapping to the middle magnetosphere, yet remain at local dawn implying influence from the solar wind.

[10] Voyager 1 observed Saturn's UV auroral emissions and radiofrequency radiation at Saturn kilometric wavelengths (SKR) during its 1980 flyby. UVS observations over several hours during a preencounter north/south map showed a factor of 5 increase in auroral emission with a peak 1–2 h, or 50° in longitude, before the maximum probability for detection of SKR [*Sandel and Broadfoot*, 1981]. The SKR was known to be modulated with a period close to that of the planet rotation, with SKR sources restricted to a broad local time range in the morning sector [*Gurnett et al.*, 1981a; *Warwick et al.*, 1981; *Kaiser et al.*, 1981]. The SKR was reported to statistically be most intense when longitude $\lambda_{SLS} = 110°$ was directed toward the Sun, implying an asymmetry in the excitation or beaming process and interaction with the solar flux or solar wind. Observations of Saturn's aurorae in January 2004 when the Cassini spacecraft was $30–33 \times 10^6$ km upstream from Saturn showed that the auroral emissions clearly brightened at the time of a large solar wind pressure increase [*Clarke et al.*, 2005; *Crary et al.*, 2005]. For this event, the solar wind pressure, velocity, and IMF were measured by Cassini approaching Saturn. The dawn side auroral emissions brightened the most, filling the polar cap, and the main oval radius decreased in proportion to the emission brightness. The SKR power measured by the Cassini RPWS instrument [*Gurnett et al.*, 2004] also increased in intensity during this event [*Kurth et al.*, 2005] after correcting for the rotational modulation. An independent analysis of SKR intensity over the six months leading up to Cassini's arrival at Saturn has found that it is positively correlated with solar wind pressure [*Rucker et al.*, 2008]. The HST event in January 2004 appeared correlated with the dynamic pressure of the solar wind, not the direction of the IMF (as dominates at the Earth), suggesting a different kind of interaction with the solar wind [*Clarke et al.*, 2005; *Crary et al.*, 2005]. The local IMF direction was known from Cassini measurements, and owing to the large tilt of Saturn the IMF was not closely aligned with the magnetic axis over this period [*Crary et al.*, 2005]. It has been proposed that the auroral brightenings are related to the rapid closure of open tail flux induced by compression of the magnetosphere [*Cowley et al.*, 2005; *Badman et al.*, 2005]. Finally, an analysis of observations of ionospheric motions measured from thermal IR H_3^+ auroral emissions indicates that Saturn's main emissions are consistent with expected subcorotational motions at the solar wind boundary, rather than near-corotation associated with plasma closer to the planet [*Stallard et al.*, 2007].

[11] It is clear that a more comprehensive data set would be required to establish the physical relationship between the solar wind and giant planet auroral emissions. Toward this goal, a large program of Hubble Space Telescope (HST) observations was scheduled, along with coordinated measurements from the New Horizons spacecraft as it flew past Jupiter and the Cassini spacecraft orbiting Saturn. In addition, solar wind conditions at the planets were estimated by propagation from near-Earth measurements. This paper presents the HST data during the 4 campaigns, with an initial discussion of the correlations of auroral activity at Jupiter and Saturn with propagated and measured solar wind conditions.

2. Data

[12] UV images of Jupiter and Saturn were obtained using the Solar Blind Channel (SBC) of the HST Advanced Camera for Surveys (ACS). The observations were concentrated in four campaigns of daily observations: one in January–February 2007 and one in February 2008 when Saturn was close to opposition, one in February–March 2007 during the New Horizons encounter with Jupiter, and one in May–June 2007 close to Jupiter opposition. Following an instrument safemode event on day of year (DOY) 27 in 2007, the first Saturn campaign was interrupted, and restarted on DOY 40–42 with UV images from the Wide Field Planetary Camera 2 (WFPC 2) at an order of magnitude lower sensitivity. These auroral power measurements have larger error bars than the ACS data, reflecting mainly a systematic uncertainty in the zero level of emission. The sub-Earth latitude on Saturn was −13° and −8° during the first and second Saturn campaigns, affording a good view of the complete southern auroral oval but a poor view of the north. Reflected solar emissions from the discs of both planets were modeled and subtracted, then the total auroral emission was measured and converted to input power. The auroral power can be related to the total power in the incident precipitating charged particles by comparison with a detailed model [*Grodent et al.*, 2001], by assuming a 10% efficiency for the production of UV emissions (multiply P_{UV} by ten for total input power). Observations of Jupiter alternated between the northern and southern poles, since Jupiter's magnetic poles and auroral ovals are offset and rotate in and out of the field of view from the Earth. A geometric correction factor has been applied to obtain the total auroral power, based on simulations of this observing geometry for an average auroral oval emission distribution, after disc modeling and subtraction were applied. Details of the observations and data reduction are given in Appendix A.

[13] A one-dimensional magnetohydrodynamic (MHD) model has been used to propagate solar wind measurements made near the Earth to conditions near Jupiter and Saturn [*Hanlon et al.*, 2004a, 2004b; *Zieger and Hansen*, 2008]. The model has high radial resolution and assumes spherical symmetry of the solar corona and solar wind. To determine the uncertainties in the propagation, an extensive validation has been carried out using ISEE3 spacecraft data propagated to Pioneers 10 and 11 and Voyagers 1 and 2 and ACE spacecraft data propagated to Ulysses near both Jupiter and Saturn [*Zieger and Hansen*, 2008]. These comparisons spanned heliocentric radii from Jupiter to Saturn and included cases near both solar minimum and solar maximum. The solar corona normally displays a well-ordered rigidly rotating sector structure at large distances during solar minimum conditions, which increases the accuracy of the extrapolation and is therefore optimal for the HST campaign. The validation study (details are given in Appendix A) showed that the propagation is most accurate near the time when the Sun-spacecraft-planet angle is small, i.e., they are in a line. Because of the 1-D nature of the propagation, the velocity is the most accurately modeled quantity, followed by the density and IMF magnitude (including the magnetic sector boundaries), while the normal component of the IMF is relatively poorly constrained. Since the velocity and density are accurately modeled, they can be used to study the correlation between solar wind pressure and planetary auroral power.

[14] By analogy to the Earth, it would be helpful to study the relationship between auroral power and the IMF strength and direction, which can be combined to estimate the dayside reconnection rate. The dayside reconnection rate can be estimated using the expression:

$$\Phi_R = vB_\perp L \cos^n\left(\frac{\theta}{2}\right), \tag{1}$$

where Φ_R is the reconnection voltage (equal to the flux transfer rate from the dayside to the tail), v is the solar wind speed, $B_\perp$ the perpendicular field strength, L a length that can reasonably be taken as some fraction of the size of the magnetosphere (modulated by the solar wind dynamic pressure), and the cosine function gives the dependence on the direction of the IMF, θ being the "clock" angle about the planetary magnetic axis [*Badman et al.*, 2005; *Nichols et al.*, 2007]. Since the IMF component B_N is poorly constrained by the propagation (as shown in Appendix A) the angle θ is poorly known, and we have thus concentrated in this paper on the solar wind pressure.

[15] It should be noted, however, that shock fronts in the solar wind at large distances from the Sun are normally accompanied by a pronounced increase in the magnitude of the IMF, and often by a polarity reversal of the IMF [*Zieger and Hansen*, 2008]. To this extent some conclusions may be drawn from the propagated solar wind data about IMF conditions at each planet. While it is possible that intervals of northward and southward field will influence reconnection rates and maybe "cusp" auroral output, it should be recognized that in general the directions of the field N and S are usually rapidly fluctuating on time scales of tens of minutes, particularly in the strong postshock compression regions. These time scales are generally shorter than the time scale for the solar wind to flow around the giant planet magnetospheres, and certainly short compared with the times scales of days required to significantly pump up the tail with open flux. One could in principle take advantage of the long time scales for solar wind flow around these planets to take a time average to improve the knowledge of B_N and θ. One could then determine the accuracy of these time average values in the propagation by the method in [*Zieger and Hansen*, 2008], and the resulting reconnection rate for comparison with auroral power. This study remains for future work.

[16] Within 50 days of the Sun-Earth-planet alignment, the model predicts arrival times of solar wind shock events within ±15 h accuracy (a one standard deviation estimate [*Zieger and Hansen*, 2008]). This applies to both sets of Saturn observations reported here and to the second set of Jupiter observations. The first set of Jupiter observations, corresponding to the New Horizons flyby, is as much as 100 days before alignment and the accuracy for this period is lower, closer to ±24 h. New Horizons (NH) measurements of the solar wind approaching Jupiter permitted us to fix the time scale for the arrival of solar wind events up to DOY 56, after which NH was in the magnetosphere and unable to detect the solar wind. The passage of Cassini into the solar wind on DOY 38 in 2008 similarly allowed us to correct the arrival time of that disturbance at Saturn. These two solar wind data sets were shifted by a constant in time based on the single measured arrival times of large events in the solar wind, and the uncertainty in timing may therefore be larger as the time from these events increases.

3. Saturn's Auroral Activity

[17] Data from the Saturn auroral images are given in Figures 1–4, with auroral images in Figures 1 and 3, summarizing the nature of the auroral activity during the January–February 2007 and February 2008 campaigns. The main oval changed in brightness and shifted in latitude, and isolated bright emission regions appeared and disappeared in less than a planet rotation period, similar to past behavior [*Trauger et al.*, 1998; *Gérard et al.*, 2004; *Clarke et al.*, 2005; *Crary et al.*, 2005; *Gérard et al.*, 2006]. Measurements of total auroral power and oval outer radius are compared with SKR power and propagated solar wind velocity and dynamic pressure in Figures 2 and 4. For both Jupiter and Saturn, solar wind forward shocks (indicated by vertical shaded regions) have been identified by the arrival time of a sharp velocity increase accompanied by a pressure increase. In the 2007 solar wind data, the propagated pressure increase sometimes did (DOY 14–15) and sometimes did not (DOY 42) lag the velocity increase. It should be pointed out that the DOY 14–15 event does not cleanly fit our definition of a forward shock, owing to the short pressure increase on DOY 14. It is clear that the general DOY 14–15 event coincided within the uncertainty with increases in both UV auroral power and SKR emission, which persisted for nearly a week, and the UV oval radius generally decreased during this period. The auroral and SKR emissions returned to a more normal level after DOY 20, on which there was a dawn side brightening of the auroral emissions. This could be analogous to the dawn storms on Jupiter, which have been reported before for

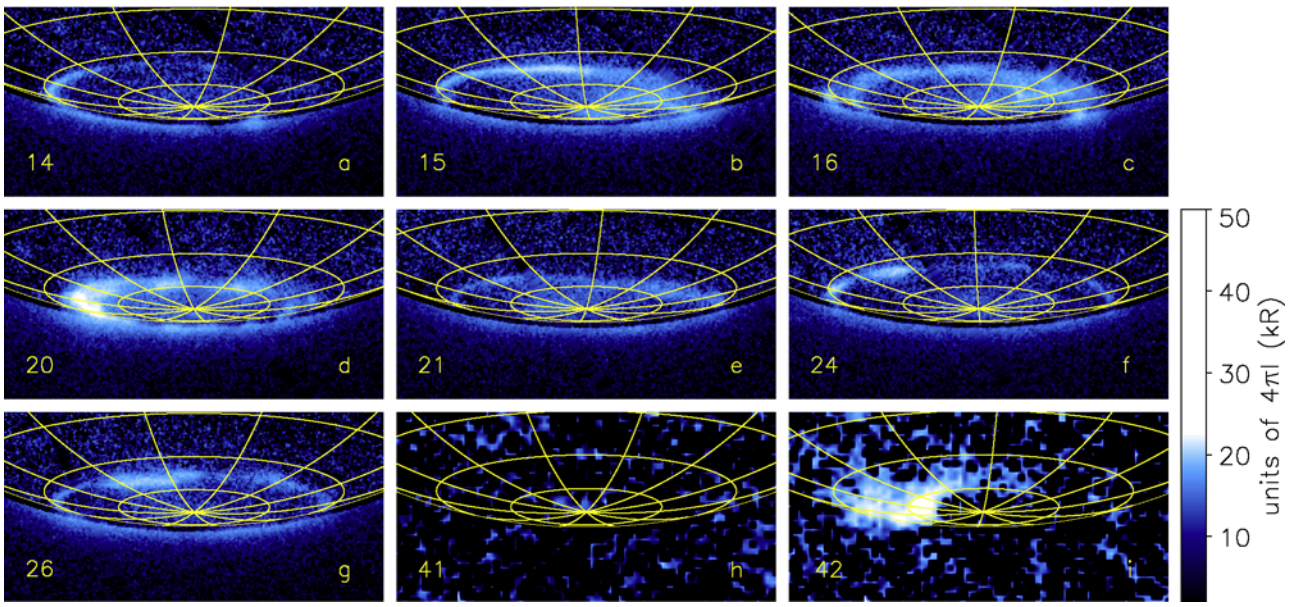

Figure 1. Sample UV images of Saturn's south pole in January–February 2007 with quiet and disturbed conditions. The left-hand number is day of year in 2007, and the part label letters correspond to the lettering at the top of Figure 2. All images are displayed with the same log intensity scale in kRayleighs, 30° lines of SLS longitude, and 10° lines of planetocentric latitude. Figures 1a–1g were obtained with ACS, with a limiting sensitivity of 1–2 kR after modeling and subtraction of reflected solar emissions. Figures 1h and 1i were taken with WFPC 2. With a limiting sensitivity of about 10 kR, these images do not show the relatively faint emissions seen in the ACS images.

Saturn [*Trauger et al.*, 1998; *Gérard et al.*, 2006]. The observations on DOY 20 were not long enough to determine if the brightest emission remained fixed at local dawn, as seen with the dawn storms on Jupiter. The solar wind pressure remained high with a slow decrease over DOY 15–20, with a reverse shock (a velocity increase with a pressure decrease) seen on DOY 19, a few hours before the dawn storm-like event. The DOY 42 event also corresponded with increased UV and SKR emissions, while the oval radius could not be accurately measured in the low-sensitivity WFPC 2 images. It is interesting to note that the dusk side of the oval filled in with emission over DOY 15–16, while the dawn side oval brightened and filled with emission on DOY 42 and to a lesser extent on DOY 20. A smaller increase in SKR emission on DOY 24 was not matched by any detected increase in auroral power, although this could be related to issues of SKR source locations compared with the location of the spacecraft (see section 5). Similarly, an isolated increase in auroral power was measured on DOY 25, although the aurora were unusually faint leading up to this return to a normal quiet brightness. On the basis of the 2007–2008 data, we found an average quiet power ~10 GW, and each case of elevated auroral power above the average level of 10 GW in the 2007 data was matched by increased SKR emission and solar wind pressure. For this Saturn campaign, there appears to be a good general correlation between auroral power, SKR emission, and solar wind pressure, both for the relatively weaker event over DOY 14/15–20 and the stronger event on DOY 42 (see later discussion).

[18] A relatively more concentrated series of ACS auroral images was obtained in the second Saturn campaign over DOY 32–48 in February 2008 (Figure 3). There were two solar wind forward shocks identified in this period, and a reverse shock arrived just hours after the last HST images. With the solar wind parameters shifted to match the Cassini measurement of the shock arrival at Saturn on DOY 38, each forward shock is consistent within the one sigma timing uncertainty with clear increases in both the auroral UV power and the SKR emission. The auroral brightening on DOY 38–39 appeared mainly along the dawn side of the oval, with an initial increase at 01 UT on DOY 38, followed by a moderate decline at 10 UT, followed by a larger brightening at 04–08 UT on DOY 39. The auroral event on DOY 44 also was concentrated on the dawn side, although for this event much of the polar region appeared filled with emission, as in January 2004. Unfortunately, for the bright emissions on DOY 39 and 44, the equatorward boundary was not well defined, and it was not possible to make reliable measurements of the oval radius. The solar wind event on DOY 48 was followed by an observed increase in SKR emission, but this occurred just after the last HST observation so that there was no measurement of any auroral brightening that may have occurred. This last event was a reverse shock, with the solar wind density decreasing at the time of a velocity increase, nonetheless there was an increase in SKR emission. In this concentrated series of HST images, especially over DOY 32–38, no other significant auroral increases were observed. There is thus no evidence for significant auroral brightenings above a level of 10–15 GW at times without solar wind events in either 2007 or 2008.

[19] These same general trends were observed in the January 2004 observations [*Clarke et al.*, 2005; *Kurth et*

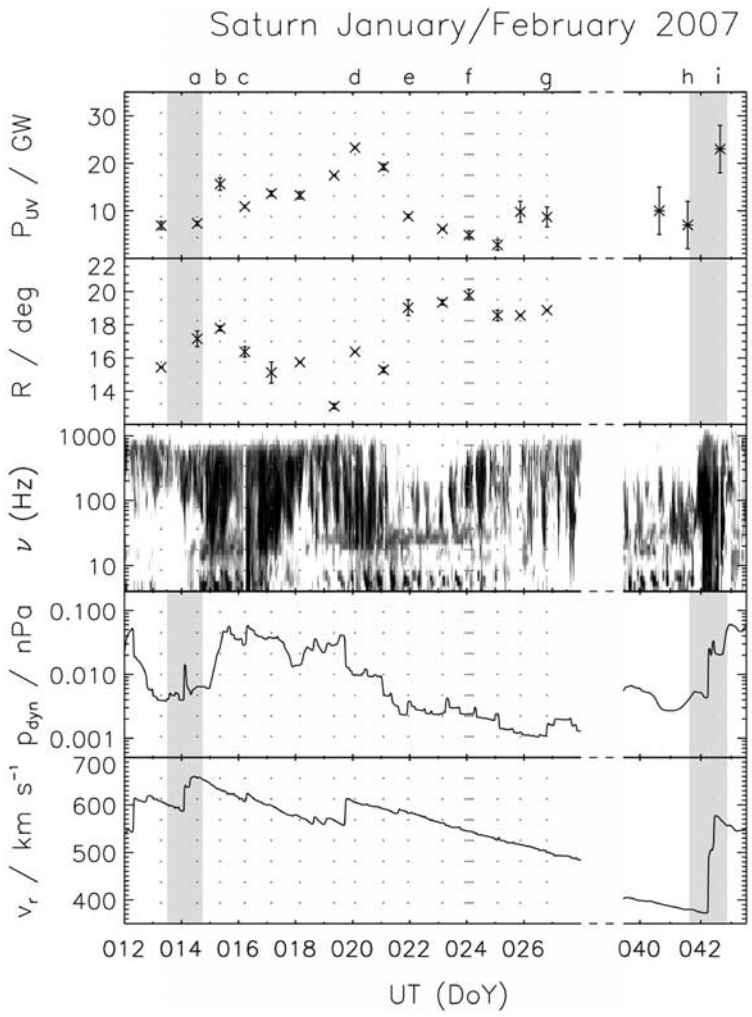

Figure 2. Total auroral power from Saturn's south polar region, best fit auroral oval radius, and SKR emission spectrum compared with propagated solar wind velocity and dynamic pressure in January–February 2007. Oval radius values were obtained by fitting a circle to the low-latitude edge of the observed auroral emissions. SKR emission measurements are from the Cassini RPWS instrument. Solar wind values were obtained by propagation from Earth-based measurements, with forward shock times $\pm 1\sigma$ uncertainties shaded.

al., 2005; *Crary et al.*, 2005], during which an increase in solar wind pressure to values of 0.02–0.04 nPa corresponded with a major auroral storm, with radiated powers of 60–80 GW (equal to 600–800 GW of input power). The first event reported here (DOY 15–22 in 2007) had a lower radiated power (15–25 GW) but lasted for seven days compared with two to three days in January 2004, although the solar wind pressure was similar during the two events. The oval radius values were also similar, with a smaller decrease over DOY 15–22 in 2007 consistent with the smaller auroral brightening. During this event, the SKR also intensified considerably, and a similar correlation was detected in January 2004 [*Kurth et al.*, 2005]. The auroral brightening on DOY 40–42 in 2007 was a larger event than the earlier brightening, although the auroral power value is relatively uncertain since the WFPC 2 did not detect the fainter emissions recorded in the ACS images. The auroral brightenings seen in February 2008 were similar in power to the 2007 events, with increases in total power of a factor of 2–3 lasting for a few hours to a couple of days, while the solar wind pressure varied by nearly 2 orders of magnitude. The event on DOY 38–39 2008 occurred following several days of low solar wind pressure, which would correspond to an inflated magnetosphere. At the time of the latter event the solar wind pressure had been elevated for 4–5 days, corresponding to a compressed magnetosphere, nonetheless the auroral brightenings on DOY 39 and 44 were of similar strength. While this is a limited sample, it appears that the auroral brightenings are better correlated with the arrival of a shock than with the integrated solar wind pressure over the preceding days.

[20] In summary, the Saturn observations covered four forward shocks and two reverse shocks. The data support a persistent increase in Saturn's auroral power and SKR emission, and decrease in the oval radius, at times of arrival

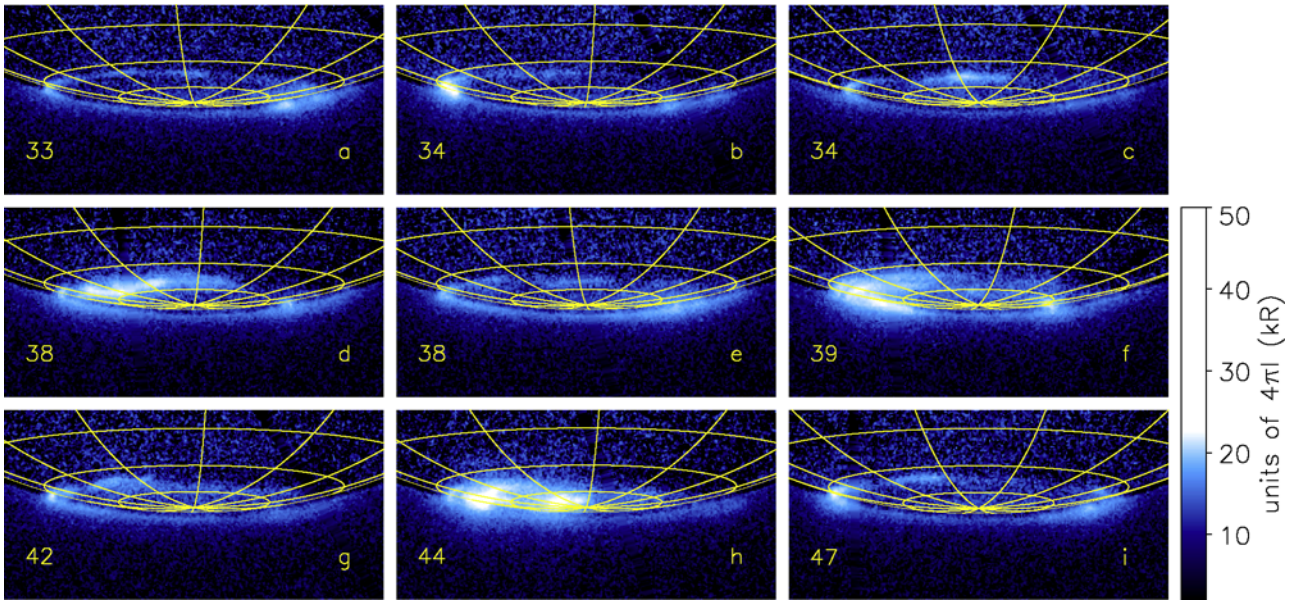

Figure 3. Sample UV images of Saturn's south pole in February 2008 with quiet and disturbed conditions. The left-hand number is day of year in 2008, and the part label letters correspond to the lettering at the top of Figure 4. Intensity scale and longitude/latitude grid are as in Figure 1. All frames were obtained with ACS, with a limiting sensitivity of 1–2 kR after modeling and subtraction of reflected solar emissions.

of increased solar wind velocity and pressure, with a much larger sample size than previously available.

4. Jupiter's Auroral Activity

[21] Similar presentations of the auroral images from Jupiter with propagated solar wind velocities and pressures are given in Figures 5–8 for the Jupiter campaigns in February–March 2007 and May–June 2007. Two forward shocks and two reverse shocks in the solar wind arrived at Jupiter during the first campaign. The first event in the propagation was a velocity and pressure increase over DOY 51–53. Measurements from the New Horizons SWAP instrument close to Jupiter found a pressure increase on DOY 53 (H. Elliott, New Horizons SWAP solar wind measurements at Jupiter encounter, paper presented at Magnetospheres of the Outer Planets 2007, Southwest Research Institute, San Antonio, Texas, 2007), consistent with the arrival of the propagated pressure increase, and the propagated data for this campaign were shifted to match this locally measured time. The auroral emissions along the main oval, both north and south, brightened slightly over DOY 51–53 then increased sharply on DOY 54, coincident with the solar wind pressure increase. The second solar wind forward shock on DOY 65 occurred at a time when there were no auroral images for nearly 2 days after its arrival, at which time the auroral brightness was not remarkable. The main oval did brighten on DOY 63, and remained bright for at least two days, during a period of low solar wind pressure. A two standard deviation shift back in time would be required for the auroral and solar wind events to coincide, and in fact taking out the overall shift in the propagated times based on the New Horizons measurement on DOY 54 would make these events coincide within a few hours. In both cases, solar wind velocity and pressure increases were coincident within the uncertainty in the propagation time, and the auroral brightenings were along the main oval. A third velocity increase on DOY 60 was accompanied by a pressure decrease (a reverse shock), and little change in auroral power was seen, although there were no images for the 2 days leading up to this event. Finally, a dawn storm event (a brightening along the main oval remaining near local dawn as the planet rotated) was observed on DOY 69, when there were no significant events in the solar wind. A solar wind velocity increase was seen 2 days earlier, but the pressure generally decreased for several days centered on this dawn storm. The solar wind arrival times would have to be shifted forward by 3 1/2 days for the dawn storm and pressure increase on DOY 65 to match, and this shift would be in addition to the shift that has been made to match the New Horizons measurements, therefore it seems unlikely that the dawn storm was related to earlier changes in the solar wind.

[22] In the second campaign, four solar wind forward shocks and two reverse shocks occurred. While there were no in situ measurements to zero out the arrival times of solar wind disturbances in this campaign, Jupiter was near opposition, with a correspondingly lower uncertainty in arrival time from the propagation. On DOY 134 and 153, forward shocks arrived at Jupiter, with moderate increases in the main oval auroral brightness seen consistent with the shock arrival times. Another forward shock late on DOY 143 arrived one day after a dawn storm auroral event was observed on DOY 142. No auroral brightening was observed on DOY 143, although a brightening lasting just a few hours cannot be ruled out owing to the spacing of the images. A correlation with the earlier dawn storm would require a two sigma shift in the arrival time of the shock.

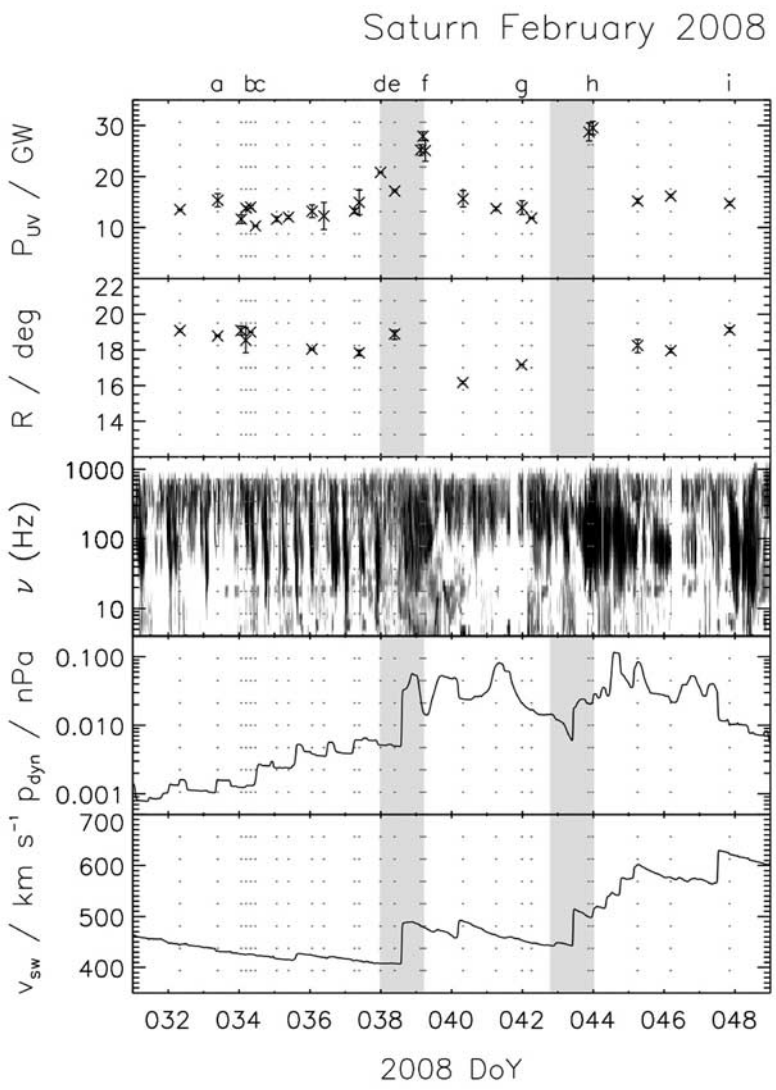

Figure 4. Total auroral power and other parameters as in Figure 2 for the February 2008 period. Solar wind values obtained by propagation from Earth-based measurements have arrival times shifted 2.6 days later to match the time when Cassini measured a strong compression of the magnetosphere on DOY 38. Times of solar wind forward shock times plus and minus 1σ uncertainties are shaded.

The remaining solar wind velocity increase on DOY 158 occurred at a time of mildly increased pressure from an already high level on DOY 156, and a general brightening of the southern aurora was observed over these two days with a maximum just after the shock arrival on DOY 158. The high solar wind pressure during this event was similar to that on DOY 134, with similar increases in auroral power during the two events. By contrast, a reverse shock on DOY 160 with steeply declining pressure occurred during a period when no auroral brightenings were observed in the following two days. An auroral brightening on DOY 149 (a dawn storm) occurred when there were no events in the solar wind for at least two days before or after. It should be noted that on several days the overall auroral power increases were due to brighter low-latitude emissions, for example, on DOY 156–157 and to a lesser extent on DOY 138.

[23] In summary, the Jupiter observations covered six solar wind forward shocks and three reverse shocks. The auroral power increased at some level during all of the forward shocks, with some uncertainty in the arrival times, while the reverse shocks showed no auroral brightenings. Dawn storms observed on DOY 69 and 149 occurred at times when there were no clear solar wind events, while the dawn storm on DOY 142 is subject to the same timing uncertainty. Overall, it appears that Jupiter's auroral activity may increase at times of solar wind forward shocks, but not at times of reverse shocks, and dawn storms may occur independently of the solar wind velocity and pressure.

5. Discussion

[24] To summarize the results, four solar wind forward shocks are presented of varying strength at Saturn, in addition to two earlier reported events in January 2004.

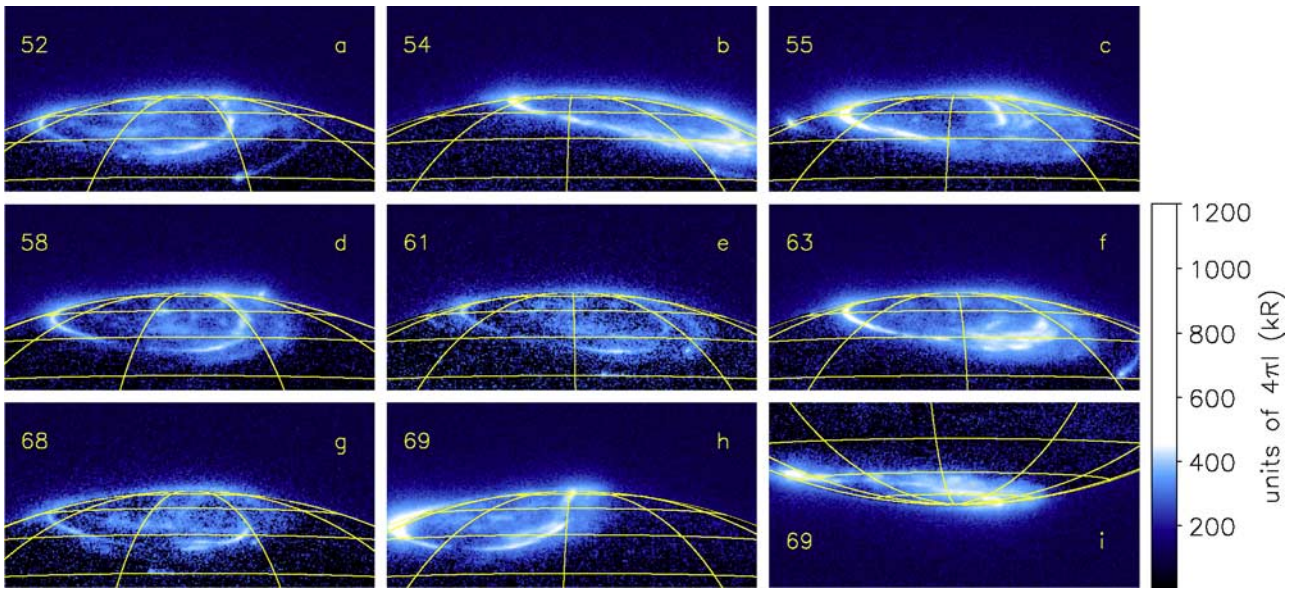

Figure 5. Sample UV images of Jupiter's aurorae with quiet and disturbed conditions during February–March 2007 observations coincident with the New Horizons flyby of Jupiter. The left-hand number is day of year in 2007, and the part label letters correspond to the lettering at the top of Figure 6. Intensity scale and longitude/latitude grid are as in Figure 1.

There is a one to one correspondence between the arrival of solar wind shocks at Saturn and increases in Saturn's auroral power and SKR emission, and decrease in the oval radius. At the times of two reverse shocks the SKR emission appeared to increase, and possibly also the UV emission although the statistics are poor. These data are consistent with a causal relationship between solar wind disturbances and auroral and SKR emission increases. At Jupiter, six

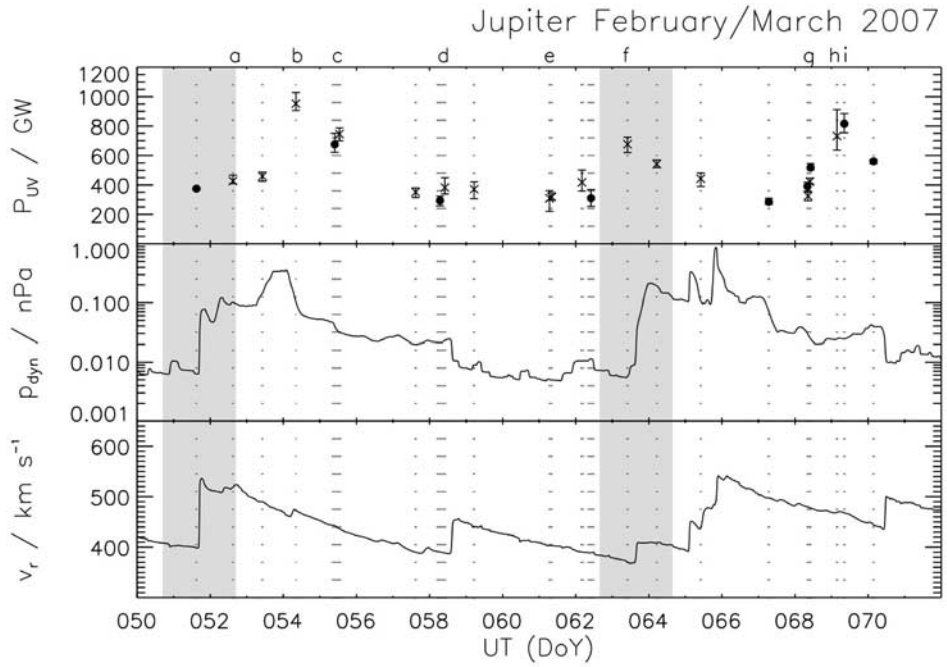

Figure 6. Total auroral power from Jupiter's north (crosses) and south (filled circles) polar regions compared with propagated solar wind velocity and dynamic pressure in February–March 2007 during the New Horizons flyby. Solar wind arrival times at Jupiter were shifted 2.1 days later than the propagation to match the time when New Horizons SWAP data measured a pressure increase on DOY 53. Auroral power values have been estimated compensating for the known variations in observing geometry from the Earth (see Appendix A). Arrival times of solar wind forward shocks are indicated by shaded regions indicating the uncertainty in propagated arrival times.

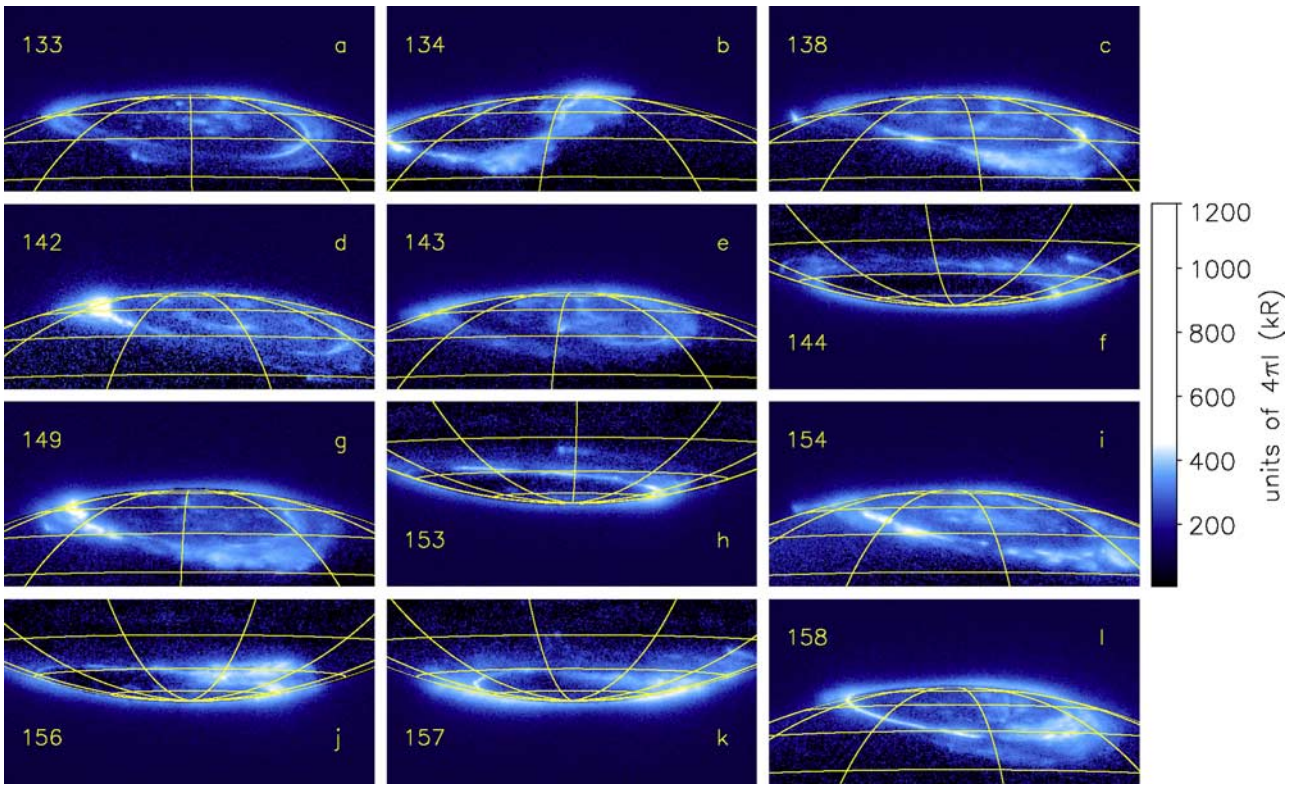

Figure 7. Composite of sample images of Jupiter's aurorae with quiet and disturbed conditions during May–June 2007 observations near Jupiter opposition. The left-hand number is day of year in 2007, and the part label letters correspond to the lettering at the top of Figure 8. Intensity scale and longitude/latitude grid are as in Figure 1.

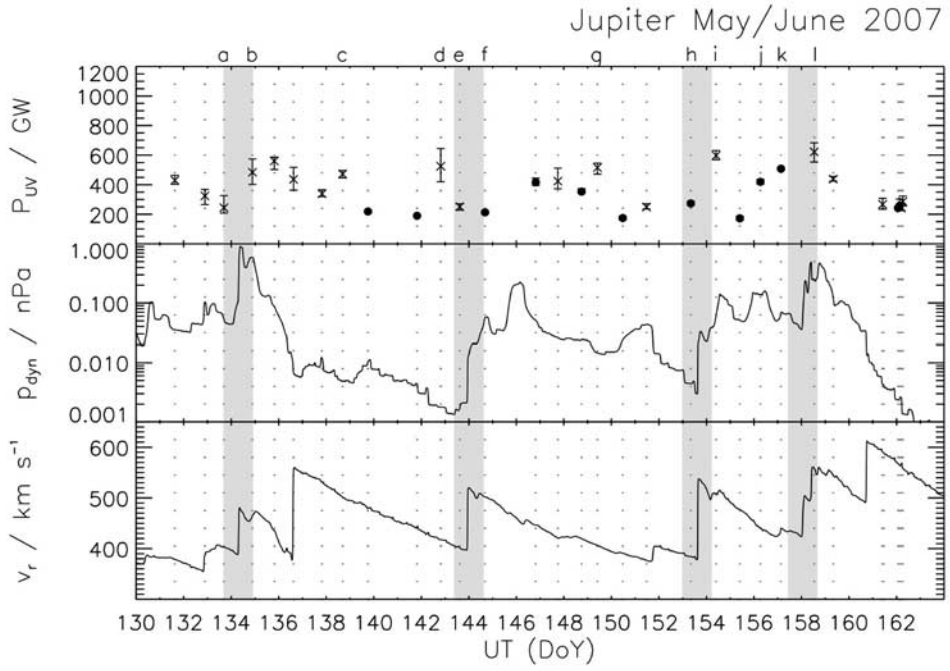

Figure 8. Total auroral power from Jupiter's north (crosses) and south (filled circles) polar regions compared with propagated solar wind dynamic pressure in May–June 2007. Arrival times of solar wind forward shocks are indicated by shaded regions as in Figure 6.

Table 1. Coefficients of Linear Correlation With Auroral Power

Auroral Observations	Solar Wind Pressure	Solar Wind Radial Velocity	SKR Power
Saturn 2007	0.22/0.51	0.39/0.40	0.30
Saturn 2008	0.60/0.85	0.58/0.61	0.02
Jupiter 1 (DOY 50–69)	0.15/0.54	0.27/0.55	n/a
Jupiter 2 (DOY 130–161)	0.45/0.51	−0.07/0.13	n/a

solar wind forward shocks and three reverse shocks are presented. The auroral power increased at some level during each of the forward shocks, subject to the uncertainty in arrival times, while no auroral brightenings were observed upon the arrival of any reverse shock. Dawn storms were observed at times with no solar wind events, suggesting an internal origin of these auroral events. The implication is that the solar wind has some causal relationship with Jovian auroral processes, while auroral increases also occur independently of changes in the solar wind.

[25] To test earlier indications that the auroral emissions at Saturn and Jupiter respond to solar wind conditions, the significance of linear correlation has been estimated between total auroral power at each planet and solar wind pressure and velocity. The linear correlation coefficients, based on the data presented in Figures 2, 4, 6, and 8, are given in Table 1. Owing to the uncertainty in the arrival time of solar wind structures from the propagation, we have listed both coefficients for the nominal arrival times plotted in Figures 2, 4, 6, and 8 and the maximum that is found if the arrival time is shifted ±2 days. The 2 day period has been chosen on the basis of the two shifts that were found necessary in comparison with nearby spacecraft measurements (+2.1 days for the February 2007 Jupiter data and +2.6 days for the February 2008 Saturn data). It can be seen from Table 1 that the maximum possible correlation of auroral power with solar wind pressure is above 0.50 for both planets when such a shift is included. Since there is no independent evidence for these shifts, these coefficients should be regarded as upper limits to the significance of the correlation. On the other hand, the true nature of the solar wind conditions at each planet may be shifted by a variable amount over each period of observation, and local measurements of the solar wind with a more accurate timing could in principle either increase or decrease the degree of correlation.

[26] The determination of a linear correlation tests the hypothesis that auroral power is linearly correlated with solar wind pressure or velocity. However, the arrival of a shock (either a compression or relaxation) may initiate processes within the magnetosphere that give rise to an auroral intensification that lasts for a longer or shorter time than the disturbed solar wind conditions are maintained. If the disturbed magnetospheric conditions settled into an equilibrium state while the solar wind pressure remained high, for example, this would decrease the significance of a linear correlation. In addition, because of the difficulty in propagating IMF conditions from 1 AU to these planets, no estimates are presented here of the IMF orientation or resulting dayside reconnection. The IMF conditions may be quite important at Jupiter and Saturn, as they are at the Earth. To the extent that the IMF markedly increases at the arrival of a shock, as consistently found in the propagations [*Zieger and Hansen*, 2008], correlations with solar wind shock arrivals could alternately indicate a dependence on the IMF and increase in dayside reconnection.

[27] Linear correlation coefficients have also been estimated between Saturn's auroral power and SKR power. Since the SKR emission is clearly modulated with the planetary rotation period, we have taken the average SKR emission over each planet rotation as a first attempt to compensate. The SKR power was first smoothed using a boxcar width of 5 h and then averaged over bins of length ∼10.82 h, centered on 180° SKR longitude, as defined by *Kurth et al.* [2008]. This is not expected to be sufficient to correct for the true geometry of Cassini measurements, for reasons given in Appendix A. Because of the changing orbital location of Cassini around Saturn, the spacecraft is known to move in and out of locations that might detect SKR sources, so that the measured intensity must be corrected for observing geometry using a model for the emission distribution to obtain the intrinsic SKR intensity [*Lamy et al.*, 2008; *Cecconi et al.*, 2009]. A more detailed analysis of the SKR emission and correlations with auroral power is the subject of the Ph.D. thesis of L. Lamy at Meudon Observatory.

[28] At Saturn, the linear correlation coefficient between auroral power and solar wind pressure is much higher for the 2008 data than for the 2007 data. In the 2007 campaign there was a sustained increase in auroral power over DOY 15–20 and a sharp increase on DOY 42, while in 2008 there was a rather broad increase in solar wind pressure over DOY 38–47 followed by two sharp auroral brightenings on DOY 38 and 43 at times of shocks. The correlation coefficient between auroral power and SKR intensity is low in both years, although in the SKR data there appear to be clear increases in SKR intensity within the rotational modulation at times of auroral increases. The significance of this correlation may change when multiple sources of SKR and their beaming patterns are taken into account. If the SKR emissions are produced in conjunction with auroral emissions, their distribution and beaming would be matched to the location of bright auroral emissions, so that the intensity measured at Cassini would depend on the location of the spacecraft with respect to the instantaneous auroral emission distribution.

[29] Another way to pose the question is to determine if the auroral power increased each time a forward shock in the solar wind arrived at Saturn. This has been the case in each event in 2007 and 2008, and also in the 2004 observations, giving a total of 6 events for which coincident increases were seen. The auroral brightenings at Saturn may be compared with the response of the Earth's aurora to solar wind velocity and pressure increases. At the Earth these normally begin with brightenings near noon, then extend around the oval to the nightside on time scales of minutes, and occur more often during southward IMF orientations. Auroral brightenings at Saturn occur most often in the dawn sector, and at times fill in the polar regions, with the region of brightest emission moving poleward of the latitude of the oval during quiet conditions. The Saturn brightenings can last for hours to days, in some cases longer than the extent of the solar wind pressure increase. The details of this interaction remain to be determined, but there are important clues to constrain the nature of the interaction in the sense of

the observed correlations and the long time scale for solar wind flow past Saturn's much larger magnetosphere.

[30] At Jupiter, the linear correlation coefficients for each campaign are lower than at Saturn, both for nominal timing and the maximum shifted correlation. In the February–March 2007 data, the solar wind pressure varied by 2 orders of magnitude, with two sharp increases followed by gradual declines, while the auroral power was generally constant to ±30% with three short-term brightenings on the order of a factor of 2 in total power. The lower correlation may be due to the different time scales for variations between the solar wind and aurora. A similar pattern was seen in the May–June 2007 data. Again, there is a question about the time scales for solar wind disturbances to influence the magnetosphere, even more so than at Saturn owing to the large size of the Jovian magnetosphere. The lower significance of a linear correlation may reflect the difference between the length of an auroral brightening and the long time scale for solar wind flow past the Jovian magnetosphere.

[31] Posing the question of whether Jupiter's auroral activity increased at the arrival of solar wind shocks, based on two historical events and six events from this campaign, the arrival of a solar wind forward shock likely corresponded with an increase in auroral power. For the events from this campaign, the brightenings were concentrated in the main oval and lower-latitude emissions. However, solar wind reverse shocks have *not* been seen to correlate with auroral brightening, based on three events from this campaign. In addition, dawn storms occur at times of quiet solar wind conditions, based on three events from this campaign. While these results are generally consistent with other indications from radio and auroral emissions [*Baron et al.*, 1996; *Zarka*, 1998; *Gurnett et al.*, 2002; *Pryor et al.*, 2005; *Nichols et al.*, 2007], they provide more detailed information on which solar wind events and auroral emissions may be causally related. With regard to the aurora, of Jupiter's three independent auroral processes (the satellite footprints, the main oval, and the polar emissions), the majority of the auroral power is from the main oval and slightly lower-latitude emissions, with up to 1/3 of the power from the polar emissions. Most of the changes in total auroral power in this study reflect changes in the main oval and lower-latitude emissions.

[32] While Saturn's main oval maps in theory to the outer magnetosphere, Jupiter's main oval maps to the middle magnetosphere, where solar wind pressure changes have a relatively smaller effect. In addition, if Jupiter's main oval is driven by currents resulting from a corotation lag of outward drifting plasma, as seems well established by both observation and theory [*Hill*, 2001; *Cowley and Bunce*, 2001; *Southwood and Kivelson*, 2001], increased solar wind pressure will decrease the rate of plasma drifting outward. This had been predicted to decrease the strength of field-aligned currents and lead to fainter auroral emissions, opposite to what is observed in the present study, although this is subject to more recent suggestions of the possible effects of supercorotation and the ionospheric flywheel [*Cowley et al.*, 2007; Hill and Gong, presented paper, 2005]. The lack of a consistent response of Jupiter's main auroral oval brightness to changing solar wind pressure from the present study suggests that the factors determining the auroral brightness are more complicated than this simple theoretical picture. The time scales and locations of auroral brightenings observed in the present study can be applied to test models of these and other processes to understand the nature of the solar wind interaction with Jupiter's magnetosphere.

[33] In summary, this paper presents a large and well sampled set of auroral observations that provide newly detailed information on the auroral activity levels on Saturn and Jupiter, and potential correlations with solar wind properties and SKR emission at Saturn. These results provide important new constraints on theories of the response of the magnetospheres of Saturn and Jupiter to changes in the solar wind.

Appendix A

A1. HST Image Reduction

[34] The HST data presented in this paper have been reduced by custom procedures at Boston University, rather than accepting the STScI pipeline. This has been done in part to make sure all processing steps are tested and understood, and in part because added or different procedures are required for images of diffuse auroral emissions. All raw HST images have undergone the following corrections as part of the BU pipeline reduction process: (1) dark count subtraction, (2) flat field response correction, (3) interpolation of values over rows of bad pixels on detector, (4) geometric distortion correction, performed in a manner to preserve the count rate per unit area, (5) rotation to place planet north up, and rescaling image size to standard distance from the Earth (8.2 AU for Saturn, 4.2 AU for Jupiter) for comparison of images taken at different times, (6) conversion to brightness units (kilo-Rayleighs per pixel) from measurement of instrument response to UV standard flux stars, assuming an auroral spectrum, (7) determination of planet center in pixel space, for mapping and projections, and (8) fitting and subtraction of a model for the solar reflected emission from the planet disc.

[35] The Solar Blind Camera (SBC) on ACS has a wavelength band pass of 115–170 nm including the H_2 Lyman bands, Werner bands, and the H Ly-α line. For clear images (F115LP), assuming an auroral spectrum, the assumed conversion factor from counts per second per pixel to kRayleigh is 0.0021. One kiloRayleigh is defined as 10^9 photons/sec from a 1 cm^2 column of atmosphere radiated isotropically into 4π steradians. Filtered images were taken in the same HST orbit with the ACS filter F125LP (>125 nm) and F140LP (>140 nm) filters. The flux conversion factors that have been used are 0.00028 cts/sec-kR per pixel for F125LP and 0.00056 cts/sec-kR per pixel for F140LP.

[36] For each image, a set of ephemeris data has been assembled from the HST data file header and from the JPL Navigation and Ancillary Information (NAIF) package. In filtered images the planet disc appears brighter than in clear images. This is because a narrow band pass has a lower response to auroral emissions, hence the flux correction factor is larger. The flux calibration is correct *only* for the auroral emissions, and *not* for reflected sunlight from the disc. The changing sky background in clear (F115) images is due to H Ly α emission from the geocorona, which increases as HST moves into the sunlit portion of its orbit.

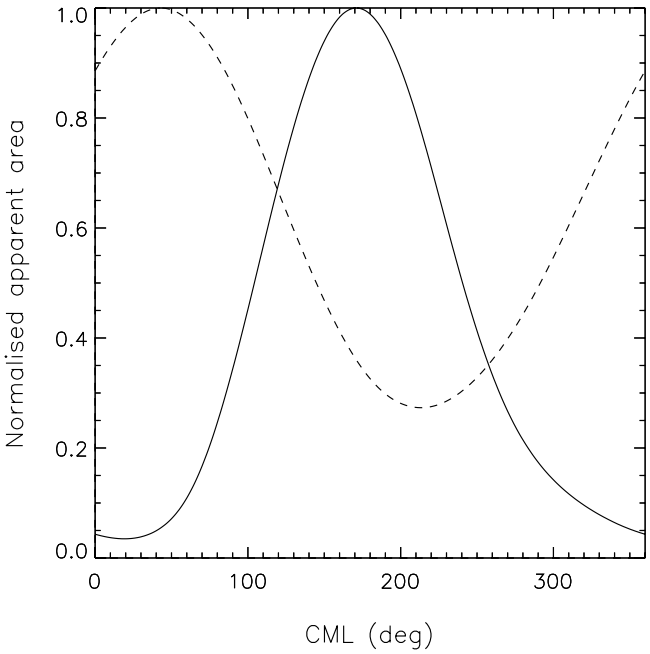

Figure A1. Geometric correction factors for the north (solid) and south (dashed) polar regions applied to Jupiter's auroral brightness data. CML is system III central meridian longitude.

The altitude extent of the auroral curtain is resolved in the images of both Jupiter and Saturn. This creates a strong bias in the apparent brightness (limb brightening) and in the apparent location of emission regions, especially close to the planet limb and in regions of extended emission. A good example of these effects can be seen in one of the daily movies where the Io footprint emission is near the planet limb. Most of the UV auroral emission is optically thin, so that limb brightening is a real effect.

[37] The center pixel location routines require manual location of the planet's center. With Saturn this is relatively easy to do, as the entire planet and inner rings appear in the field of view. A simulated image of the rings with known center is shifted and differenced from each image until the difference frame is minimized. For Jupiter images the center location is relatively more uncertain, as only a fraction of the planet appears in the field of view. The north/south mapping is determined from the location of the lower edge of the auroral emission curtain from the far side of the planet limb, this altitude corresponds to the homopause hydrocarbon absorption and is assumed to be 240 km above the 1 bar level at Jupiter and 650 km at Saturn. The east/west mapping is relatively more uncertain, and a simulated planet limb is fit by eye to the sunlit terminator. Estimated uncertainties in the planet center location for Jupiter are 3 pixels north/south and 4 pixels east/west, and for Saturn are 2 pixels north/south and 2 pixels east/west. One pixel is 0.025 arc sec, compared with the angular resolution of 0.08 arc sec determined from ACS images of bright UV stars. Note that a given uncertainty in pixels corresponds to very different distances in km on the planet, depending on the distance from the limb.

[38] At each planet there are reflected solar continuum emissions from the planet disc, which vary with latitude and longitude and are fainter in the polar regions owing to absorption by complex molecules that are derived from the hydrocarbon photochemistry driven by the bright auroral emissions. These emissions can be seen without auroral emissions in images taken with a long wavelength blocking filter F165LP, and these images have been used to develop and test a model for the solar reflected emission distribution that has then been scaled and subtracted from each auroral image. The fitting procedure includes deriving the best fit Minnaert coefficients for the center to limb variations as functions of angles to both the Sun and the observer, and including a north/south intensity variation which changes with time. We have found that the north/south variation for each campaign is reasonably stable, while a new one must be estimated for each campaign. The uncertainty in auroral powers based on the disc subtraction is 10%.

[39] At Jupiter a correction for intrinsic auroral brightness as a function of the longitude of the planet is required, since the auroral zones rotate with the planet in and out of the line of sight from the Earth. These corrections, applied separately for the north and south aurora, have been estimated by taking an average brightness distribution of the auroral emissions from each pole, then simulating by projection the view from the Earth as a function of longitude. The correction values that have been applied to the data are plotted in Figure A1. The detailed schedule of the observations is given in Figures A2 and A3 in a block diagram format, along with additional information on Jupiter in Figures 5 and 7 about the CML range of the planet.

[40] Reduced image files in.fits format and movies of the daily images can be downloaded from the Planetary Atmospheres and Space Science group Web site at Boston University: http://www.bu.edu/csp/PASS/main.html.

A2. SKR Data Reduction

[41] The SKR is recorded by the High Frequency Receiver (HFR) of the RPWS experiment on board the Cassini spacecraft. This appendix briefly summarizes SKR data processing and highlights the presence of nonauroral low-frequency emissions ($f \leq 40$ kHz) as well as SKR visibility effects observed in the final dynamic spectra. These points have been described and discussed in detail [*Lamy et al.*, 2008]. Goniopolarimetric inversions applied to Cassini-RPWS-HFR radio measurements allow one to retrieve the physical parameters of the wave, i.e., the flux of the Poynting vector and polarization state [*Cecconi and Zarka*, 2005].

[42] During the HST observations of January 2007 and 2008, the HFR recorded radio observations in many different operating modes resulting in a heterogeneous data set (different integration times, frequency resolution and scale). Radio data have consequently been organized in regular time-frequency maps (or dynamic spectra) with a time resolution of 3 min and a relatively coarse frequency ramp between 3.5 kHz and 1500 kHz. Since the RPWS electric antenna non only detects the SKR but also non-SKR electromagnetic and electrostatic emissions as well as radio frequency interference (RFI), a way to extract the SKR is to select circularly polarized events. A detection threshold of 20% of the circular polarization degree has been applied to

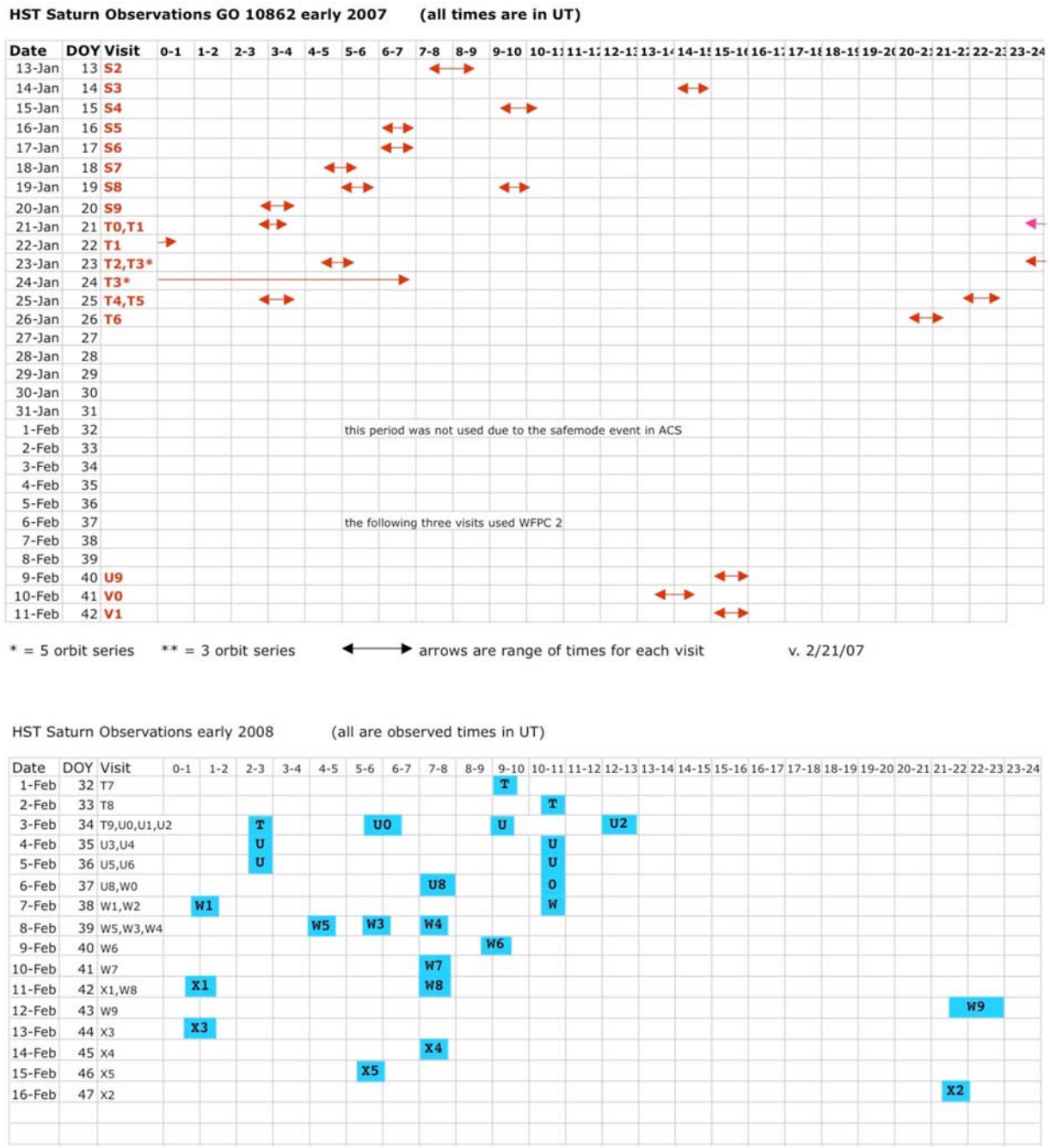

Figure A2. Schedule of HST observations of Saturn in (top) 2007 and (bottom) 2008.

each individual event to perform this selection. Data gaps resulting from this selection (e.g., RFI horizontal lines) have been specifically processed to rebuild most of the signal. SKR fluxes from 100 to 300 kHz have then been calibrated in units of W m^{-2} Hz^{-1} and normalized to 1 AU, leading to dynamic spectra such as those displayed in Figures 2 and 4 of the main text.

[43] The broadband SKR is not the only highly circularly polarized emission observed by the HFR. Narrowband low-frequency emissions [*Gurnett et al.*, 1981b] also appear in dynamic spectra for frequencies lower than 40–50 kHz. The component between 3 kHz and 10 kHz corresponds to the narrowband myriametric emission (n-SMR) investigated by *Louarn et al.* [2007]. The component between 10 kHz and 40–50 kHz displays different characteristics noted by *Lamy et al.* [2008] and deserves a further extensive study. In both cases, contrary to the dominant SKR, low-frequency emissions are not auroral emissions and should not be considered in the comparative analysis between the SKR and the UV aurorae.

[44] The SKR is known to be emitted via the Cyclotron Maser Instability along a thin hollow cone whose axis is aligned with the local magnetic field and widely opened (aperture angle of $\sim 70^{\circ}$). A major consequence of this

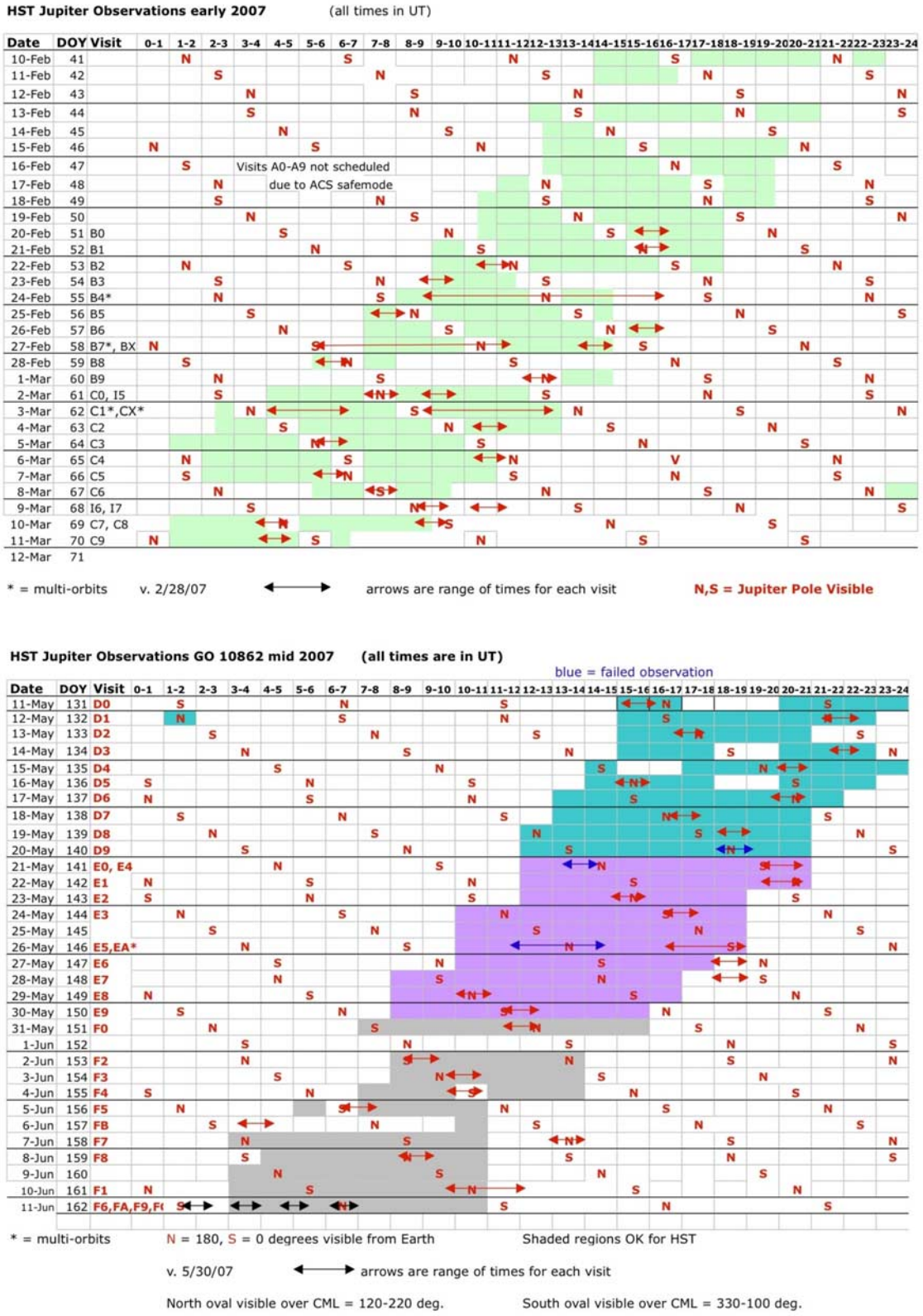

Figure A3. Schedule of HST observations of Jupiter in early and mid-2007.

strong anisotropy results in the observation of a small fraction of all emitting radio sources: the spacecraft can only detect a source when it is located in its beam [*Cecconi et al.*, 2009]. Furthermore, this anisotropy is responsible for many visibility effects directly observed in the dynamic spectra. Two of them clearly appear during the intervals studied in this article. First, the frequency extent of the SKR spectrum as well as its intensity largely depend on Cassini's

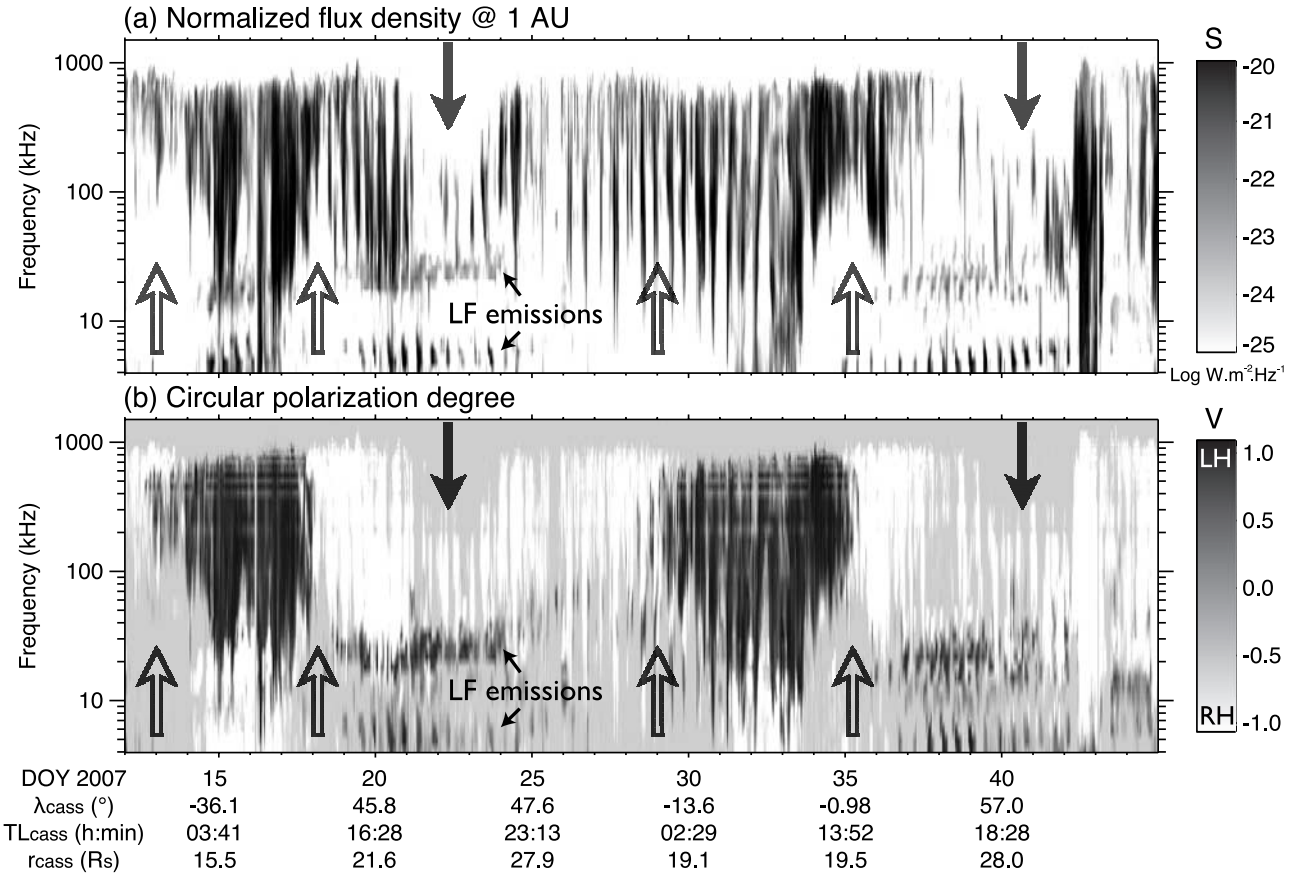

Figure A4. Dynamic spectra of (a) flux density S (in W m^{-2} Hz^{-1}) normalized to 1 AU and (b) normalized degree of circular polarization V, with each corresponding intensity bar on the right-hand side. The displayed interval (from DOY 13 to 45) includes that of the 2007 HST campaign (from DOY 13 to 42). The dynamic spectra not only show the intense broadband SKR but also nonauroral low-frequency emission below 40 kHz. Moreover, as a consequence of the SKR anisotropy combined with the changing location of the spacecraft, two typical visibility effects appear in dynamic spectra. When Cassini crosses the equatorial plane, the frequency extent of the SKR spectrum decreases (empty arrows), whereas when Cassini passes at high northern latitudes (>55°), the SKR highest and lowest frequencies disappear (full arrows). Both visibility effects directly affect the measured SKR power.

latitude, and are at a minimum when Cassini is located above Saturn's equator (Figure A4). Each crossing of the ring plane naturally results in smaller spectral extent and lower intensity, as observed for days 13 and 35 of year 2007 and days 39 and 42 of 2008. Second, the SKR lowest and highest frequencies have been observed to disappear when Cassini reaches high northern latitudes. This feature is clearly observed on days 21 to 24 and 39 to 42 of 2007. Such visibility biases strongly affect the SKR detected power (implying variations of ~2 orders of magnitude) which is thus only indicative of the intrinsic SKR emitted power and should be used very carefully. In such conditions, relatively high values of correlation coefficients computed in this article between SKR and UV aurora appear likely to have a high significance.

A3. Solar Wind Propagation

[45] The solar wind propagation method presented in this paper has been used extensively to study solar wind conditions in the outer solar system [*Hanlon et al.*, 2004a, 2004b; *Prangé et al.*, 2004; *Bunce et al.*, 2008]. To determine the accuracy with which the model predicts the solar wind, a detailed validation of the model has been conducted using ICEE3, ACE, Pioneer, Voyager, Ulysses and Cassini data. Every detail of the model including the method for calculating the solar wind as well as the validation results is given by *Zieger and Hansen* [2008]. In this appendix we review the results of the two validation studies presented in that paper so that the reader of this paper can understand more completely the accuracy of solar wind predictions presented here.

[46] In the validation paper two different measures of the accuracy of the propagation method are presented. The first is a correlation of the propagated solar wind with spacecraft data. Because of the one-dimensional nature of the propagation, the prediction efficiency is expected to be best at the time of apparent opposition. The apparent opposition is defined here as the time of opposition of Earth and a given planet or any other body plus the solar wind propagation time from Earth to the body at an average speed of 500 km/s. Figure A5 shows the correlation between the propagated solar wind and the spacecraft data for all available spacecraft

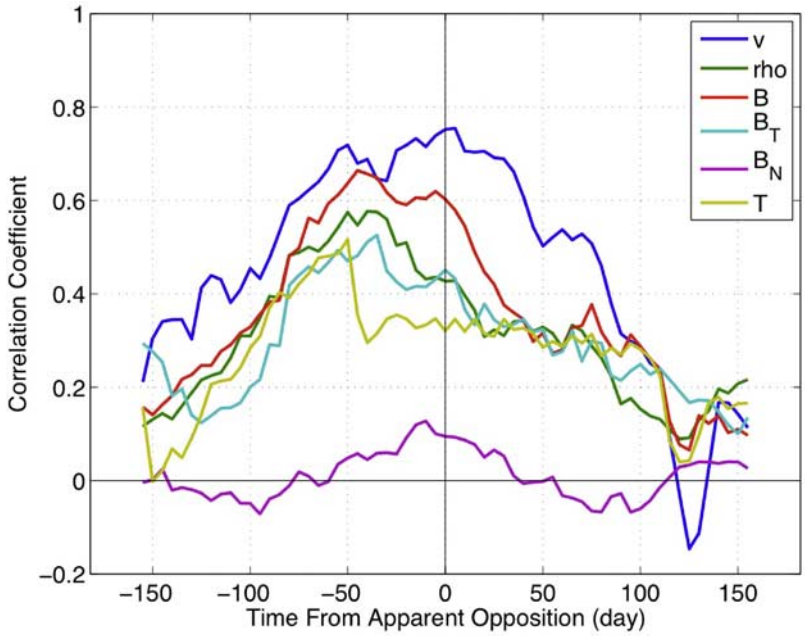

Figure A5. Prediction efficiency of solar wind variables as a function of time from apparent opposition for solar minimum conditions.

during years of solar minimum. It can be seen that the most reliable predictions are expected within 75 days from apparent opposition. Correlations between predicted and observed solar wind variables outside of this range are considerably lower but still statistically significant. The most accurately predicted solar wind variable is the solar wind velocity. The IMF magnitude, density and the tangential component of IMF (B_T) are the next most accurate in the respective order (the propagation is carried out in the RTN coordinate system). Note that the predictions of the normal component of IMF (B_N) are very poor as shown by the hardly significant correlations between predicted and observed B_N.

[47] As a second measure of the accuracy of the model we have studied the arrival time of discontinuities in the solar wind dynamic pressure. We choose this quantity to study shock arrival because the dynamic pressure is thought to play a significant role in driving the magnetospheres of Jupiter and Saturn. For this study, each year of spacecraft data has been divided into ten hour segments. This is short enough that only one discontinuity is typically present in each segment while at the same time being long enough for good statistics. In each segment we calculate a lagged cross correlation with the solar wind propagation. The lag times that maximize the correlation represent the error in the arrival time of the discontinuity. During the years of solar minimum conditions, the median time lags of dynamic pressure enhancements, typically shocks in corotating interaction regions (CIR), are very close to zero especially within 75 days from apparent opposition (see Figure A6). The interquartile range (marked with error bars in Figure A6) tells us that 50% of the shock arrival times are within the time lag range between −15 and 10 h at the time of apparent opposition during years of solar minimum. The distributions of shock arrival times become significantly wider as we move farther away from the apparent opposition, but no statistically significant deviation from zero is observed in the median time lags, at least during years of solar minimum. At solar maximum, however, predicted shocks tend to delay by at least 10 h (not shown here), which is a systematic error implying extra shock acceleration in the real solar wind.

A4. Estimation of Correlation Coefficients

[48] There are a number of different approaches that can be taken to estimate the degree of linear correlation between auroral power and solar wind pressure or velocity, which correspond to testing different assumptions about what might be the nature of the physical connection. In this section we present different approaches that were tried to estimate the possible degree of correlation between auroral power and other parameters.

A4.1. Data Sampling

[49] We have included auroral power values averaged over each HST visit, which can range from 1 h for a single HST orbit visit to 7–8 h for a multiple orbit visit. Within each visit, the auroral power was not seen to change by a large amount, and to avoid excessively weighting the significance of times when we had multiple orbits, we have used the auroral power for each visit as a single point in the correlation analysis. For the propagated solar wind values, we have smoothed the data by a 1 h running mean to match the HST orbital period of observations. Testing has shown that this smoothing has not significantly changed the correlation coefficients.

A4.2. Direct Comparison of Values Versus Log of Change From Mean Value

[50] The *Baron et al.* [1996] paper gave a comparison of the changes in the log of IR auroral power and solar wind

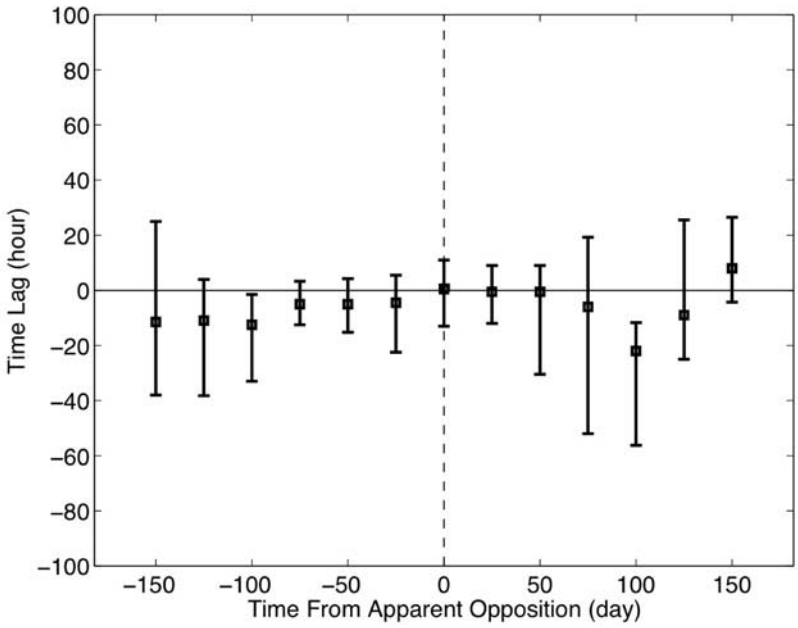

Figure A6. Spread of shock arrival time distributions as a function of time from apparent opposition during solar minimum.

pressure, and did not quote the degree of correlation between the direct values. For a comparison with their work, we have determined the degree of correlation between the difference from the mean value of the log of each quantity. The degree of correlation for the nominal timing is generally much lower than for the comparison of the quantities presented in the main text, while the maximum coefficient based on shifting the solar wind arrival time is generally similar to the values presented in the paper. Since no uncertainties were given by Baron et al. for the arrival times of solar wind events, it is not possible to judge the significance of solar wind arrival time shifts in their data.

A4.3. Shift in Timing of SW Data by ±2 Sigma to Get Max Correlation

[51] As described in the text, owing to the uncertainty in the arrival time of solar wind structures from the propagation, we have listed both coefficients for the nominal arrival time and the maximum that is found if the arrival time is shifted ±2 days. The 2 day period has been chosen on the basis of the two shifts that were found necessary in comparison with nearby spacecraft measurements.

[52] **Acknowledgments.** This work is based on observations with the NASA/ESA Hubble Space Telescope, obtained at the Space Telescope Science Institute, which is operated by AURA for NASA. Work in Boston was supported by grant HST-GO-10862.01-A from the Space Telescope Science Institute to Boston University. J.C.G. and D.G. are supported by the Belgian Fund for Scientific Research (FNRS) and by the PRODEX program of ESA. L.L., P.Z., and B.C. acknowledge support from the Centre National d'Études Spatiales in France. We acknowledge helpful discussions with Tom Hill, Alex Dessler, George Parks, Heather Elliott, Benoit Hubert, Margaret Kivelson, Fran Bagenal, and Dave McComas.

[53] Wolfgang Baumjohann thanks the reviewers for their assistance in evaluating this paper.

References

Akasofu, S.-I. (1964), The development of the auroral substorm, *Planet. Space Sci.*, *12*, 273–282, doi:10.1016/0032-0633(64)90151-5.

Arridge, C. S., C. T. Russell, K. K. Khurana, N. Achilleos, S. W. H. Cowley, M. K. Dougherty, D. J. Southwood, and E. J. Bunce (2008), Saturn's magnetodisc current sheet, *J. Geophys. Res.*, *113*, A04214, doi:10.1029/2007JA012540.

Badman, S. V., E. J. Bunce, J. T. Clarke, S. W. H. Cowley, J.-C. Gérard, D. Grodent, and S. E. Milan (2005), Open flux estimates in Saturn's magnetosphere during the January 2004 Cassini-HST campaign, and implications for reconnection rates, *J. Geophys. Res.*, *110*, A11216, doi:10.1029/2005JA011240.

Ballester, G. E., et al. (1996), Time-resolved observations of Jupiter's far-UV aurora: Comparison of WFPC2 and IUE, *Science*, *274*, 409–413, doi:10.1126/science.274.5286.409.

Baron, R. L., T. Owen, J. Connerney, T. Satoh, and J. Harrington (1996), Solar wind control of Jupiter's auroras, *Icarus*, *120*, 437–442, doi:10.1006/icar.1996.0063.

Barrow, C. H., F. Genova, and M. D. Desch (1986), Solar wind control of Jupiter's decametric radio emission, *Astron. Astrophys.*, *165*, 244–250.

Boudouridis, A., E. Zesta, R. Lyons, P. C. Anderson, and D. Lummerzheim (2003), Effect of solar wind pressure pulses on the size and strength of the auroral oval, *J. Geophys. Res.*, *108*(A4), 8012, doi:10.1029/2002JA009373.

Brittnacher, M., M. Wilber, M. Fillingim, D. Chua, G. Parks, J. Spann, and G. Germany (2000), Global auroral response to a solar wind pressure pulse, *Adv. Space Res.*, *25*, 1377–1385, doi:10.1016/S0273-1177(99)00647-X.

Bunce, E. J., et al. (2008), Origin of Saturn's aurora: Simultaneous observations by Cassini and the Hubble Space Telescope, *J. Geophys. Res.*, *113*, A09209, doi:10.1029/2008JA013257.

Cecconi, B., and P. Zarka (2005), Model of a variable radio period for Saturn, *J. Geophys. Res.*, *110*, A12203, doi:10.1029/2005JA011085.

Cecconi, B., L. Lamy, P. Zarka, R. Prangé, W. S. Kurth, and P. Louarn (2009), Goniopolarimetric study of the revolution 29 perikrone using the Cassini Radio and Plasma Wave Science instrument high-frequency radio receiver, *J. Geophys. Res.*, *114*, A03215, doi:10.1029/2008JA013830.

Clarke, J. T., et al. (1998), Hubble Space Telescope imaging of Jupiter's UV aurora during the Galileo orbiter mission, *J. Geophys. Res.*, *103*(E9), 20,217–20,236, doi:10.1029/98JE01130.

Clarke, J. T., D. Grodent, S. Cowley, E. Bunce, J. Connerney, and T. Satoh (2004), Jupiter's aurora, in *Jupiter: The Planet, Satellites, and Magnetosphere*, pp. 639–670, Cambridge Univ. Press, Cambridge, U. K.

Clarke, J. T., et al. (2005), Morphological differences between Saturn's ultraviolet aurorae and those of Earth and Jupiter, *Nature*, *433*, 717–719, doi:10.1038/nature03331.

Chua, D., G. Parks, M. Brittnacher, W. Peria, G. Germany, J. Spann, and C. Carlson (2001), Energy characteristics of auroral electron precipitation:

A comparison of substorms and pressure pulse related auroral activity, *J. Geophys. Res.*, *106*(A4), 5945–5956, doi:10.1029/2000JA003027.

Connerney, J. E. P., M. H. Acuña, and N. F. Ness (1983), Currents in Saturn's magnetosphere, *J. Geophys. Res.*, *88*(A11), 8779–8789, doi:10.1029/JA088iA11p08779.

Cowley, S. W. H., and E. J. Bunce (2001), Origin of the main auroral oval in Jupiter's coupled magnetosphere-ionosphere system, *Planet. Space Sci.*, *49*, 1067–1088, doi:10.1016/S0032-0633(00)00167-7.

Cowley, S. W. H., and E. J. Bunce (2003), Corotation-driven magnetosphere-ionosphere coupling currents in Saturn's magnetosphere and their relation to the auroras, *Ann. Geophys.*, *21*, 1691–1707.

Cowley, S. W. H., and M. Lockwood (1992), Excitation and decay of solar wind-driven flows in the magnetospere-ionosphere system, *Ann. Geophys.*, *10*, 103–115.

Cowley, S. W. H., E. J. Bunce, and R. Prangé (2003), Saturn's polar ionospheric flows and their relation to the main auroral oval, *Ann. Geophys.*, *21*, 1–16.

Cowley, S. W. H., S. V. Badman, E. J. Bunce, J. T. Clarke, J.-C. Gérard, D. Grodent, C. M. Jackman, S. E. Milan, and T. K. Yeoman (2005), Reconnection in a rotation-dominated magnetosphere and its relation to Saturn's auroral dynamics, *J. Geophys. Res.*, *110*, A02201, doi:10.1029/2004JA010796.

Cowley, S. W. H., J. D. Nichols, and D. J. Andrews (2007), Modulation of Jupiter's plasma flow, polar currents, and auroral precipitation by solar wind-induced compressions and expansions of the magnetosphere: A simple theoretical model, *Ann. Geophys.*, *25*, 1433–1463.

Crary, F., et al. (2005), Solar wind dynamic pressure and electric field as the main factors controlling Saturn's aurorae, *Nature*, *433*, 720–722, doi:10.1038/nature03333.

Dungey, J. W. (1961), Interplanetary magnetic field and the auroral zones, *Phys. Rev. Lett.*, *6*, 47–48, doi:10.1103/PhysRevLett.6.47.

Elphinstone, R. D., J. S. Murphree, and L. L. Cogger (1996), What is a global auroral substorm?, *Rev. Geophys.*, *34*(2), 169–232, doi:10.1029/96RG00483.

Gérard, J.-C. (2006), Saturn's auroral morphology and activity during quiet magnetospheric conditions, *J. Geophys. Res.*, *111*, A12210, doi:10.1029/2006JA011965.

Gérard, J.-C., D. Grodent, J. Gustin, A. Saglam, J. T. Clarke, and J. T. Trauger (2004), Characteristics of Saturn's FUV aurora observed with the Space Telescope Imaging Spectrograph, *J. Geophys. Res.*, *109*, A09207, doi:10.1029/2004JA010513.

Gladstone, G. R., et al. (2002), A pulsating auroral X-ray hot spot on Jupiter, *Nature*, *415*, 1000–1003, doi:10.1038/4151000a.

Goertz, C. (1978), Energization of charged particles in Jupiter's outer magnetosphere, *J. Geophys. Res.*, *83*, 3145–3150, doi:10.1029/JA083iA07p03145.

Grodent, D., J. H. Waite Jr., and J.-C. Gérard (2001), A self-consistent model of the Jovian auroral thermal structure, *J. Geophys. Res.*, *106*(A7), 12,933–12,952, doi:10.1029/2000JA900129.

Grodent, D., J. T. Clarke, J. Kim, J. H. Waite Jr., and S. W. H. Cowley (2003a), Jupiter's main auroral oval observed with HST-STIS, *J. Geophys. Res.*, *108*(A11), 1389, doi:10.1029/2003JA009921.

Grodent, D., J. T. Clarke, J. H. Waite Jr., S. W. H. Cowley, J.-C. Gérard, and J. Kim (2003b), Jupiter's polar auroral emissions, *J. Geophys. Res.*, *108*(A10), 1366, doi:10.1029/2003JA010017.

Gurnett, D. A., W. S. Kurth, and F. Scarf (1981a), Plasma waves near Saturn: Initial results from Voyager 1, *Science*, *212*, 235–239, doi:10.1126/science.212.4491.235.

Gurnett, D. A., W. Kurth, and F. Scarf (1981b), Narrowband electromagnetic emissions from Saturn's magnetosphere, *Nature*, *292*, 733–737, doi:10.1038/292733a0.

Gurnett, D. A., et al. (2002), Control of Jupiter's radio emission and aurorae by the solar wind, *Nature*, *415*, 985–987, doi:10.1038/415985a.

Gurnett, D., et al. (2004), The Cassini radio and plasma wave investigation, *Space Sci. Rev.*, *114*, 395–463, doi:10.1007/s11214-004-1434-0.

Gustin, J., S. W. H. Cowley, J.-C. Gérard, G. R. Gladstone, D. Grodent, and J. T. Clarke (2006), Characteristics of Jovian morning bright FUV aurora from Hubble Space Telescope/Space Telescope Imaging Spectrograph imaging and spectral observations, *J. Geophys. Res.*, *111*, A09220, doi:10.1029/2006JA011730.

Hanlon, P. G., M. K. Dougherty, N. Krupp, K. C. Hansen, F. J. Crary, D. T. Young, and G. Tóth (2004a), Dual spacecraft observations of a compression event within the Jovian magnetosphere: Signatures of externally triggered supercorotation?, *J. Geophys. Res.*, *109*, A09S09, doi:10.1029/2003JA010116.

Hanlon, P. G., M. K. Dougherty, R. J. Forsyth, M. J. Owens, K. C. Hansen, G. Tóth, F. J. Crary, and D. T. Young (2004b), On the evolution of the solar wind between 1 and 5 AU at the time of the Cassini Jupiter flyby: Multispacecraft observations of interplanetary coronal mass ejections including the formation of a merged interaction region, *J. Geophys. Res.*, *109*, A09S03, doi:10.1029/2003JA010112.

Hill, T. W. (2001), The Jovian auroral oval, *J. Geophys. Res.*, *106*(A5), 8101–8107, doi:10.1029/2000JA000302.

Hill, T. W. (2004), Auroral structures at Jupiter and Earth, *Adv. Space Res.*, *33*, 2021–2029, doi:10.1016/j.asr.2003.05.037.

Hubert, B., M. Palmroth, T. V. Laitinen, P. Janhunen, S. E. Milan, A. Grocott, S. W. H. Cowley, T. Pulkkinen, and J.-C. Gérard (2006), Compression of the Earth's magnetotail by interplanetary shocks directly drives transient magnetic flux closure, *Geophys. Res. Lett.*, *33*, L10105, doi:10.1029/2006GL026008.

Kaiser, M. (1993), Time-variable magnetospheric radio emissions from Jupiter, *J. Geophys. Res.*, *98*, 18,757–18,765, doi:10.1029/93JE01279.

Kaiser, M., M. Desch, and A. Lecacheux (1981), Saturnian kilometric radiation: Statistical properties and beam geometry, *Nature*, *292*, 731–733, doi:10.1038/292731a0.

Kurth, W. S., et al. (2005), An Earth-like correspondence between Saturn's ultraviolet auroral features and radio emission, *Nature*, *433*, 722–725, doi:10.1038/nature03334.

Kurth, W. S., T. F. Averkamp, D. A. Gurnett, J. B. Groene, and A. Lecacheux (2008), An update to a Saturnian longitude system based on kilometric radio emissions, *J. Geophys. Res.*, *113*, A05222, doi:10.1029/2007JA012861.

Ladreiter, H., and Y. Leblanc (1989), Jovian hectometric radiation—Beaming, source extension, and solar wind control, *Astron. Astrophys.*, *226*, 297–310.

Lamy, L., P. Zarka, B. Cecconi, R. Prangé, W. S. Kurth, and D. A. Gurnett (2008), Saturn kilometric radiation: Average and statistical properties, *J. Geophys. Res.*, *113*, A07201, doi:10.1029/2007JA012900.

Livengood, T. A., W. Moos, G. Ballester, and R. Prangé (1992), Jovian ultraviolet auroral activity, 1981–1991, *Icarus*, *97*, 26–45, doi:10.1016/0019-1035(92)90055-C.

Louarn, P., et al. (2007), Observation of similar radio signatures at Saturn and Jupiter: Implications for the magnetospheric dynamics, *Geophys. Res. Lett.*, *34*, L20113, doi:10.1029/2007GL030368.

McPherron, R. L. (1970), Growth phase of magnetospheric substorms, *J. Geophys. Res.*, *75*, 5592–5599, doi:10.1029/JA075i028p05592.

Meurant, M., J.-C. Gerard, C. Block, B. Hubert, and V. Coumans (2004), Propagation of electron and proton shock-induced aurora and the role of the interplanetary magnetic field and solar wind, *J. Geophys. Res.*, *109*, A10210, doi:10.1029/2004JA010453.

Nichols, J. D., E. J. Bunce, J. T. Clarke, S. W. H. Cowley, J.-C. Gérard, D. Grodent, and W. R. Pryor (2007), Response of Jupiter's UV auroras to interplanetary conditions as observed by the Hubble Space Telescope during the Cassini flyby campaign, *J. Geophys. Res.*, *112*, A02203, doi:10.1029/2006JA012005.

Prangé, R., P. Zarka, G. E. Ballester, T. A. Livengood, L. Denis, T. D. Carr, F. Reyes, S. J. Bame, and H. W. Moos (1993), Correlated variations of UV and Radio emissions during an outstanding Jovian auroral event, *J. Geophys. Res.*, *98*, 18,779–18,791, doi:10.1029/93JE01802.

Prangé, R., G. Chagnon, M. G. Kivelson, T. A. Livengood, and W. Kurth (2001), Temporal monitoring of Jupiter's auroral activity with IUE during the Galileo mission: Implications for magnetospheric processes, *Planet. Space Sci.*, *49*, 405–415, doi:10.1016/S0032-0633(00)00161-6.

Prangé, R., L. Pallier, K. C. Hansen, R. Howard, A. Vourlidas, R. Courtin, and C. Parkinson (2004), An interplanetary shock traced by planetary auroral storms from the Sun to Saturn, *Nature*, *432*, 78–81, doi:10.1038/nature02986.

Pryor, W. R., et al. (2005), Cassini UVIS observations of Jupiter's auroral variability, *Icarus*, *178*, 312–326, doi:10.1016/j.icarus.2005.05.021.

Rucker, H. O., et al. (2008), Saturn kilometric radiation as a monitor for the solar wind?, *Adv. Space Res.*, *42*, 40–47, doi:10.1016/j.asr.2008.02.008.

Sandel, B. R., and A. Broadfoot (1981), Morphology of Saturn's aurora, *Nature*, *292*, 679–682, doi:10.1038/292679a0.

Skinner, T. E., S. Durrance, P. Feldman, and W. Moos (1984), IUE observations of longitudinal and temporal variations in the Jovian auroral emission, *Astrophys. J.*, *278*, 441–448, doi:10.1086/161809.

Siscoe, G. L., and T. S. Huang (1985), Polar cap inflation and deflation, *J. Geophys. Res.*, *90*, 543–547, doi:10.1029/JA090iA01p00543.

Sittler, E. C., Jr., M. F. Blanc, and J. D. Richardson (2006), Proposed model for Saturn's auroral response to the solar wind: Centrifugal instability model, *J. Geophys. Res.*, *111*, A06208, doi:10.1029/2005JA011191.

Southwood, D., and M. Kivelson (2001), A new perspective concerning the influence of the solar wind on Jupiter, *J. Geophys. Res.*, *106*, 6123–6130, doi:10.1029/2000JA000236.

Stallard, T., C. Smith, S. Miller, H. Melin, M. Lystrup, A. Aylward, N. Achilleos, and M. Dougherty (2007), Saturn's auroral/polar H_3^+ infrared emission, *Icarus*, *191*, 678–690, doi:10.1016/j.icarus.2007.05.016.

Trauger, J. T., et al. (1998), Saturn's hydrogen aurora: Wide field and planetary camera 2 imaging from the Hubble Space Telescope, *J. Geophys. Res.*, *103*(E9), 20,237–20,244, doi:10.1029/98JE01324.

Waite, J. H., et al. (2001), An auroral flare at Jupiter, *Nature*, *410*, 787–789, doi:10.1038/35071018.

Warwick, J., et al. (1981), Planetary radio astronomy observations from Voyager 1 near Saturn, *Science*, *212*, 239–243, doi:10.1126/science.212.4491.239.

Zarka, P. (1998), Auroral radio emissions at the outer planets: Observations and theories, *J. Geophys. Res.*, *103*(E9), 20,159–20,194, doi:10.1029/98JE01323.

Zieger, B., and K. C. Hansen (2008), Statistical validation of a solar wind propagation model from 1 to 10 AU, *J. Geophys. Res.*, *113*, A08107, doi:10.1029/2008JA013046.

E. Bunce, S. W. H. Cowley, and T. Stallard, Department of Physics and Astronomy, University of Leicester, Leicester LE1 7RH, UK.

B. Cecconi, L. Lamy, and P. Zarka, LESIA, Observatoire de Paris, UPMC, CNRS, Université Paris Diderot, F-92190 Meudon, France.

J. T. Clarke, J. Duval, J. Nichols, and S. Wannawichian, Center for Space Physics, Boston University, Boston, MA 02215, USA. (jclarke@bu.edu)

F. Crary, G. R. Gladstone, and K. Retherford, Southwest Research Institute, San Antonio, TX 78238, USA.

M. Dougherty, Blackett Laboratory, Imperial College, London SW7 2BZ, UK.

J.-C. Gérard and D. Grodent, LPAP, Université de Liège, B-4000 Liège, Belgium.

K. C. Hansen and B. Zieger, AOSS Department, University of Michigan, Ann Arbor, MI 48109, USA.

W. Kurth, Department of Physics and Astronomy, University of Iowa, Iowa City, IA 52242, USA.

D. Mitchell, Johns Hopkins University Applied Physics Laboratory, Laurel, MD 20723, USA.

W. Pryor, Department of Science, Central Arizona College, Coolidge, AZ 85228, USA.